Structural and conformational dynamics of supercooled polymer melts: Insights from first-principles theory and simulations

Song-Ho Chong,[1] Martin Aichele,[2,3] Hendrik Meyer,[3] Matthias Fuchs,[4] and Jörg Baschnagel[3]
[1]*Institute for Molecular Science, Okazaki 444-8585, Japan*
[2]*Institut für Physik, Johannes Gutenberg–Universität, 55099 Mainz, Germany*
[3]*Institut Charles Sadron, 6 rue Boussingault, 67083 Strasbourg, France*
[4]*Fachbereich Physik, Universität Konstanz, 78457 Konstanz, Germany*
(Received 16 July 2007; published 30 November 2007)

We report on quantitative comparisons between simulation results of a bead-spring model and mode-coupling theory calculations for the structural and conformational dynamics of a supercooled, unentangled polymer melt. We find semiquantitative agreement between simulation and theory, except for processes that occur on intermediate length scales between the compressibility plateau and the amorphous halo of the static structure factor. Our results suggest that the onset of slow relaxation in a glass-forming melt can be described in terms of monomer caging supplemented by chain connectivity. Furthermore, a unified atomistic description of glassy arrest and of conformational fluctuations that (asymptotically) follow the Rouse model emerges from our theory.

DOI: 10.1103/PhysRevE.76.051806 PACS number(s): 61.25.Hq, 64.70.Pf, 61.20.Lc

I. INTRODUCTION

Polymeric melts can often be cooled down easily to vitrify into disordered solids. It is an important challenge for first-principles approaches to develop an understanding of this technologically important process. In polymer science a further important challenge is to derive well-known models of chain transport and relaxation in melts [1]. In a melt, excluded volume interactions and chain connectivity cause subdiffusive segment motion, (approximately) described by the Rouse and reptation models, which consider a single chain in an effective field [2]. The challenge consists in deriving these models from microscopic interactions.

In this paper, we propose an atomistic interpretation of the structural and conformational dynamics of a bead-spring model for an unentangled polymer melt [3,4] by quantitatively comparing simulation and first-principles calculations. On the one hand, this explains the onset of the viscous slowing down, ultimately leading to kinetic arrest into an amorphous solid (the glass transition) [5–8]. On the other hand, we find Rouse-like motion for very large chain length N, and also explain characteristic deviations from pure Rouse behavior for finite N. Our theory does not describe entanglements [9] because we start from isotropic, correlated monomer collisions which give rise to the "cage effect" in dense fluids, but vanish in the limit of infinitely thin chains where only topological constraints (entanglements) are present. We aim to describe fundamental consequences of the local steric packing in dense melts of flexible polymers and thus, in a first step, neglect chemical structure like torsional degrees of freedom; for simulation studies of the glass transition using chemically realistic models, see, e.g., Refs. [6,7,10].

Our approach is based on an extension of the mode-coupling theory (MCT) for the glass transition [11] to polymer systems. MCT predicts structural arrest—also referred to as the idealized liquid-glass transition—driven by the mutual blocking of a particle and its neighbors at a critical temperature T_c which is located above the glass-transition temperature T_g. Although complete structural arrest at T_c is not observed in experiments and simulations, extensive tests of the theory carried out so far above T_c suggest that MCT deals properly with some essential features of the structural relaxation in glass-forming liquids [12,13].

Our extension of the MCT to polymer systems will be done following the site formalism [14]. In this formalism, each polymer molecule is divided into interaction sites, corresponding to monomers or segments, and the dynamics as well as the static structure of polymers are characterized by site-site correlation functions. For chains consisting of N monomers, the site-site correlation functions comprise $O(N^2)$ elements, and handling them is a formidable task for long chains. A key assumption of our atomistic theory [15] is the replacement of the site-specific intermolecular surroundings of a monomer by an averaged one (equivalent-site approximation [14,15]), while keeping the full intramolecular site dependence. For the statics this approximation has been verified by simulation for wavelengths around the average segment separation for a bead-spring model of a polymer melt [16]. Here we extend the test by presenting a quantitative comparison of the theory for collective and single-chain dynamics with molecular-dynamics (MD) simulations. This test requires as only input the average static structure factor $S(q)$, the average intrachain structure factor $w(q)$, and the site-resolved intrachain structure factors $w_{ab}(q)$ to be defined below. These quantities are directly determined from the simulation [16]. Such a fully quantitative comparison has been done only recently, even for systems of simpler constituents [17]. It is motivated by successful MCT fits of the simulation data for our model [4].

It might be appropriate at the start to summarize the philosophy of our approach for developing an atomistic theory of the slow structural dynamics in polymer melts, combining simulation and MCT. We aim to derive first-principles results for measurable quantities like intermediate scattering functions and mean-square displacements. Within MCT, such averaged information on the structural relaxation can be ob-

tained from equilibrium structural input up to a single unknown parameter, the time scale parameter, which needs to be found by matching theory and simulation at one time instant (we will choose the final relaxation time of density fluctuations at the wavelength corresponding to the average segment separation for this purpose). We argue that quantities obtained by averaging, assuming homogeneity, should be studied first to characterize macromolecular motion, postponing consideration of heterogeneities and molecular or segmental variations to future, more detailed studies. A central question of our investigation—besides whether such an approach is feasible at all—is what static information is required or sufficient to explain key features of macromolecular motion. Therefore, we consider a simple polymer model without chemical detail for which the required static input can be obtained with high precision, and the theoretical predictions for the dynamics, calculated without adjustable parameters, can be compared with simulation results [17]. We expect to uncover fundamental mechanisms also present in real polymer melts, for which, however, more complex static information than is necessary here might be required as input to a theory for the dynamics.

The paper is organized as follows. Section II introduces the model polymer system to be considered in the present paper. In Sec. III, we briefly review static properties of the model. Implications from the analysis of the static properties will be employed in Sec. IV to develop a tractable theory for polymer dynamics. In Sec. V, theoretical predictions on structural and conformational dynamics of the model are compared with simulation results. The paper is summarized in Sec. VI with some concluding remarks. Appendix A is devoted to the derivation of the basic equations of motion, and Appendix B to the derivation of the Rouse model based on our microscopic approach.

II. MODEL

We study a bead-spring model of linear chains, each containing $N=10$ monomers of mass m [3,4,8,18]. This is a model for highly flexible polymers, and is among the simplest models exhibiting glassy arrest and polymer specific dynamic anomalies. All monomers interact via a truncated and shifted Lennard-Jones (LJ) potential

$$U_{\mathrm{LJ}}(r)=\begin{cases}4\varepsilon_{\mathrm{LJ}}[(\sigma_{\mathrm{LJ}}/r)^{12}-(\sigma_{\mathrm{LJ}}/r)^{6}]+C, & r<2r_{\min},\\ 0, & r\geq 2r_{\min}.\end{cases} \tag{1}$$

In the following, all the quantities are expressed in LJ units with the unit of length σ_{LJ}, the unit of energy $\varepsilon_{\mathrm{LJ}}$ (setting Boltzmann's constant $k_{\mathrm{B}}=1$), and the unit of time $(m\sigma_{\mathrm{LJ}}^2/\varepsilon_{\mathrm{LJ}})^{1/2}$. The constant $C=127/4096$ is chosen so that $U_{\mathrm{LJ}}(r)$ vanishes continuously at $r=2r_{\min}$ with $r_{\min}=2^{1/6}$ being the minimum position of the nontruncated potential. In addition, successive monomers in a chain interact via a finitely extensible nonlinear elastic (FENE) potential [19]

$$U_{\mathrm{FENE}}(r)=-\frac{k}{2}R_0^2\ln\left[1-\left(\frac{r}{R_0}\right)\right], \tag{2}$$

with $R_0=1.5$ and $k=30$. The superposition of the LJ and FENE potentials leads to a steep effective bond potential with a sharp minimum at $r_{\mathrm{b}}=0.9606$.

For this model we carried out MD simulations of polymer melts at constant pressure p and constant temperature T. (The polymer melts comprise 100–120 chains, depending on temperature.) The MD simulations were performed in two steps [3,8]. For each T, the volume of the simulation box is first determined in an isobaric simulation at $p=1$. Then, this volume is kept fixed and the simulations are continued in the canonical ensemble using the Nosé-Hoover thermostat. (The choice of this thermostat does not influence the relaxation dynamics of the melt [3,8].) The simulations were carried out for the temperature range $0.47\leq T\leq 1$, corresponding to monomer densities $0.91\leq\rho_{\mathrm{m}}\leq 1.04$. The lowest simulated temperature is slightly above $T_{\mathrm{c}}^{\mathrm{MD}}\approx 0.45$, the MCT critical temperature as determined from the MD simulation (cf. Sec. IV D). Before all measurements, each state point (T,ρ_{m}) is fully equilibrated (the chains are allowed to diffuse several times over the distance corresponding to their radius of gyration). For each state point, all quantities are averaged over 150–200 independent time origins. A more detailed description of the simulation technique and simulation results for the model can be found in Refs. [3,4,8,18].

III. SUMMARY OF STATIC PROPERTIES

The static structural and conformational properties of our model have been analyzed in detail in Ref. [16]. In this section, we briefly review some of the main results of Ref. [16], which help us to develop a tractable theory for polymer dynamics.

A. Static structure factors

Let us consider a polymer melt of n chains, consisting of N identical monomers, in a volume V. We denote by $\rho=n/V$ the chain density. The static collective density fluctuations at the monomer level can most naturally be characterized by the monomer-monomer (or site-site) static structure factors

$$S_{ab}(q)=\frac{1}{n}\langle\rho_a(\mathbf{q})^*\rho_b(\mathbf{q})\rangle, \tag{3}$$

defined in terms of the coherent monomer density fluctuations for wave vector $\mathbf{q}$,

$$\rho_a(\mathbf{q})=\sum_{i=1}^{n}\exp(i\mathbf{q}\cdot\mathbf{r}_i^a)\quad(a=1,\ldots,N). \tag{4}$$

Here $\langle\cdot\rangle$ denotes the canonical averaging for temperature T, and $\mathbf{r}_i^a$ represents the position of the ath monomer in the ith chain. Since the melt is spatially homogeneous and isotropic, the structure factors depend only on the modulus of the wave vector, $q=|\mathbf{q}|$. One can split $S_{ab}(q)$ into intrachain and interchain parts,

$$S_{ab}(q) = w_{ab}(q) + \rho h_{ab}(q), \tag{5}$$

in which the intrachain contribution is given by

$$w_{ab}(q) = \frac{1}{n}\left\langle \sum_{i=1}^{n} \exp[-i\mathbf{q}\cdot(\mathbf{r}_i^a - \mathbf{r}_i^b)] \right\rangle, \tag{6}$$

and the interchain contribution by

$$\rho h_{ab}(q) = \frac{1}{n}\left\langle \sum_{i\neq j}^{n} \exp[-i\mathbf{q}\cdot(\mathbf{r}_i^a - \mathbf{r}_j^b)] \right\rangle. \tag{7}$$

These contributions reveal static correlations between monomers belonging to the same chain or to different chains, respectively.

Commonly, not these site-resolved quantities, but structure factors averaged over all monomer pairs (a,b) are discussed. For instance, we obtain the collective structure factor of the melt by

$$S(q) \equiv \frac{1}{N}\sum_{a,b=1}^{N} S_{ab}(q) = \frac{1}{nN}\langle \rho_{\mathrm{tot}}(\mathbf{q})^* \rho_{\mathrm{tot}}(\mathbf{q})\rangle, \tag{8}$$

which can be represented in terms of the total monomer density fluctuations (the second equality in the above equation),

$$\rho_{\mathrm{tot}}(\mathbf{q}) \equiv \sum_{a=1}^{N} \rho_a(\mathbf{q}) = \sum_{i=1}^{n}\sum_{a=1}^{N} \exp(i\mathbf{q}\cdot\mathbf{r}_i^a). \tag{9}$$

The average $S(q)$ can also be decomposed into intrachain and interchain parts,

$$S(q) = w(q) + \rho_{\mathrm{m}} h(q), \tag{10}$$

where $\rho_{\mathrm{m}} = N\rho$ denotes the monomer density, and

$$w(q) = \frac{1}{N}\sum_{a,b=1}^{N} w_{ab}(q), \quad h(q) = \frac{1}{N^2}\sum_{a,b=1}^{N} h_{ab}(q). \tag{11}$$

The intrachain contribution $w(q)$ is often called the "form factor" in the polymer literature [2,20].

Figure 1 shows the simulation results for $S(q)$ of our model at $T=0.47$, 0.70, and 1, which are representative temperatures in the investigated range $0.47 \leq T \leq 1.0$. In this T interval, the collective structure of the melt is typical of a dense disordered system. Due to the weak compressibility of the melt, $S(q)$ is small in the $q \to 0$ limit. As q increases, $S(q)$ increases toward a maximum, which occurs around $q^*=6.9$ in our model. The corresponding length scale $2\pi/q^*$ is associated with the average segment separation, which is of the order of the effective monomer diameter (=1 in the reduced units). Thus, the dominant contribution to $S(q^*)$ comes from the amorphous packing in neighbor shells around a monomer. Upon lowering T, Fig. 1 indicates that the packing becomes tighter, which is reflected by the increased height of the peak $S(q^*)$ and by the shift of its position q^* to larger values. Such changes of $S(q)$ at $q \approx q^*$ reflect the interchain correlations since the intrachain structure factor $w(q)$ was found to be nearly T independent [16].

In addition to monomer density fluctuations, the static spatial arrangement of the center of mass (c.m.) of chains

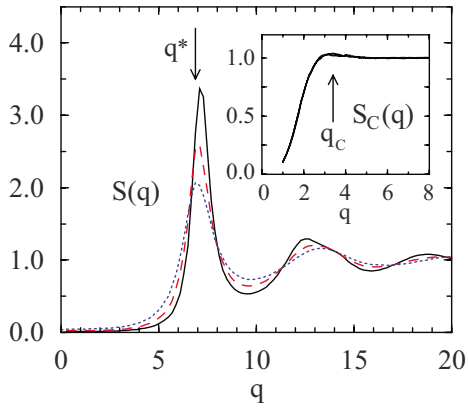

FIG. 1. (Color online) Collective static structure factor $S(q)$ of the melt as a function of the modulus of the wave vector q for temperatures $T=0.47$ (solid line), 0.70 (dashed line), and 1 (dotted line). $S(q)$ exhibits a maximum around $q^*=6.9$ whose position is indicated by an arrow. The inset shows $S_C(q)$, the static structure factor of the chain's center of mass, for $T=0.47$, 0.70, and 1. There is practically no temperature dependence in $S_C(q)$, and the three curves cannot be distinguished from each other. $S_C(q)$ exhibits a weak maximum at $q_C=3.4$ whose position is indicated by an arrow.

and its T dependence might be of interest. The c.m.-c.m. static structure factor is defined by

$$S_C(q) = \frac{1}{n}\left\langle \sum_{i,j=1}^{n} \exp[-i\mathbf{q}\cdot(\mathbf{R}_i - \mathbf{R}_j)] \right\rangle, \tag{12}$$

where $\mathbf{R}_i$ denotes the c.m. position of the ith chain. The inset of Fig. 1 shows the simulation result for $S_C(q)$. It is seen that $S_C(q)$ is fairly featureless: outside the small-q regime reflecting the low compressibility of the melt, $S_C(q)$ quickly approaches the ideal gas behavior, $S_C(q)=1$. There is a tiny peak at $q_C \approx 3.4$, whose height is, in contrast to that of $S(q)$, practically T independent.

One understands from Fig. 1 that the most pronounced T dependence in the static structure occurs in $S(q)$ around q^* which reflects interchain monomer correlations. This implies that the slowing down of the dynamics of our model upon lowering T cannot result from static c.m.-c.m. or intrachain correlations, but should be driven by interchain correlations at the monomer level, i.e., by the nearest neighbors that are not directly bonded to each other. As we will see, this is one of the principal predictions of our theory, according to which the coherent dynamics close to q^* enslaves all other dynamics, including the c.m. and single-chain conformational dynamics.

B. Equivalent-site approximation

In Ref. [16], particular attention was paid to the dependence of static correlation functions on the position of the monomer along the chain backbone to understand to what extent specific monomer-monomer correlations deviate from the average behavior. Since the site-site static correlation functions are necessary input quantities for the mode-coupling approach based on the site formalism, the compari-

son of the monomer-monomer correlation functions with their monomer-averaged counterparts can suggest suitable approximations and thus help develop a tractable theory. In this and the next subsections, we summarize such approximations, which will be employed in Sec. IV.

Let us introduce the site-site direct correlation function $c_{ab}(q)$ via the site-site Ornstein-Zernike equation [21]

$$h_{ab}(q) = \sum_{x,y=1}^{N} w_{ax}(q)c_{xy}(q)[w_{yb}(q) + \rho h_{yb}(q)]. \quad (13)$$

This is a generalized Ornstein-Zernike equation in which intrachain correlations are accounted for through $w_{ab}(q)$; it also serves as the defining equation of the direct correlation function in terms of $w_{ab}(q)$ and $S_{ab}(q)$,

$$\rho c_{ab}(q) = w_{ab}^{-1}(q) - S_{ab}^{-1}(q). \quad (14)$$

Here $X_{ab}^{-1}(q)$ ($X=w$ or S) denotes the (a,b) element of the inverse of the matrix $\mathbf{X}(q)$.

The difficulty in dealing with the site-site correlation functions arises from the dependence on the indices (a,b). Such functions consisting of $O(N^2)$ elements cannot easily be handled for large N. One can argue, however, that, for long polymers, chain end effects for interchain correlation functions should be small, suggesting that all sites of a homopolymer can be treated equivalently. (This simplification is exact for a ring homopolymer.) This equivalent-site approximation is usually invoked for $c_{ab}(q)$, i.e.,

$$c(q) = c_{ab}(q) \quad \text{(equivalent-site approximation)}. \quad (15)$$

Equation (15) represents the principal idea of the polymer reference interaction site model (PRISM) theory developed by Schweizer, Curro, and co-workers [14].

Substituting Eq. (15) into Eq. (13) and then taking the summation $\Sigma_{a,b}$ of the resulting equation, one gets the following scalar equation, called the PRISM equation, in terms of the averaged quantities defined in Eq. (11):

$$h(q) = w(q)c(q)[w(q) + \rho_{\mathrm{m}} h(q)]. \quad (16)$$

Equation (16) provides the following expression for $c(q)$:

$$\rho_{\mathrm{m}} c(q) = 1/w(q) - 1/S(q), \quad (17)$$

in terms of the average $w(q)$ and $S(q)$.

The validity of the equivalent-site approximation (15) has been examined for our model by comparing $c_{ab}(q)$ obtained from Eq. (14) with $c(q)$ from Eq. (17), with the quantities on the right-hand sides of these equations directly determined from simulations (see Fig. 5 of Ref. [16]). It has been demonstrated that the approximation is well satisfied, except for functions involving the chain ends. This result suggests that, for our model, a theory for the melt dynamics can be derived by assuming Eq. (15) without introducing a large error [22].

C. Additional ring approximation

Besides $c_{ab}(q)$, the static structure factors $S_{ab}(q)$ are necessary input quantities for the MCT based on the site formalism (see Sec. IV). Thus, the equivalent-site approximation (15) alone is insufficient to obtain a tractable theory since the specific monomer-position dependence still remains in $S_{ab}(q)$. This is obvious in view of the following relation:

$$S_{ab}(q) = [\{\mathbf{I} - \rho \mathbf{w}(q)\mathbf{c}(q)\}^{-1}\mathbf{w}(q)]_{ab}, \quad (18)$$

which can be derived from Eqs. (5) and (13). Here $\mathbf{I}$ denotes the unit matrix. Thus, even with the assumption $c_{ab}(q) = c(q)$, a site dependence of $S_{ab}(q)$ results from chain connectivity, i.e., from the matrix structure of $w_{ab}(q)$. Therefore, it is desirable to have an additional approximation which simplifies the treatment of $S_{ab}(q)$.

Remembering that the equivalent-site approximation (15) is exact for a ring polymer, we will derive an additional approximation for linear chains based on another exact relation for rings. We will then examine the validity of this approximation in our simulation.

A prominent feature of the site-site structure factor for a ring polymer is that $\tilde{S}_a(q) \equiv \Sigma_{b=1}^{N} S_{ab}(q)$ is independent of a, and the relation $\tilde{S}_a(q) = (1/N)\Sigma_{a=1}^{N} \tilde{S}_a(q) = S(q)$ holds; the second equality follows from Eq. (8). Furthermore, from the identity $\Sigma_{x,b} S_{ax}^{-1}(q) S_{xb}(q) = 1$, we also have $\tilde{S}_a^{-1}(q) \equiv \Sigma_{b=1}^{N} S_{ab}^{-1}(q) = 1/S(q)$. In view of these exact relations for a ring polymer, let us introduce the following approximations for linear chains:

$$\tilde{S}_a(q) \equiv \sum_{b=1}^{N} S_{ab}(q) \approx S(q), \quad (19)$$

$$\tilde{S}_a^{-1}(q) \equiv \sum_{b=1}^{N} S_{ab}^{-1}(q) \approx \frac{1}{S(q)}. \quad (20)$$

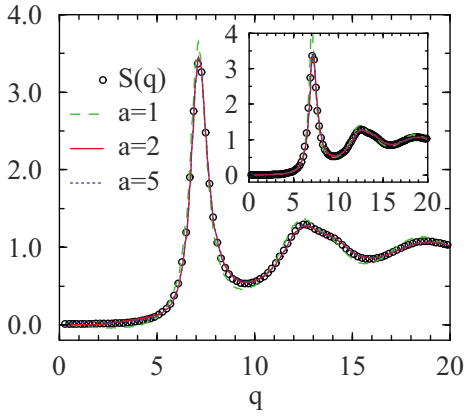

FIG. 2. (Color online) Comparison of the static structure factor $S(q)$ (circles) with the site-dependent static structure factors $\tilde{S}_a(q)$ for $a=1$ (dashed line), 2 (solid line), and 5 (dotted line). The inset compares $S(q)$ (circles) with $1/\tilde{S}_a^{-1}(q)$ for $a=1$ (dashed line), 2 (solid line), and 5 (dotted line). (The dotted lines for $a=5$ in the main panel and in the inset are not clearly visible since they almost agree with the solid lines for $a=2$.) $\tilde{S}_a(q)$ and $\tilde{S}_a^{-1}(q)$ are defined by the first equality of Eqs. (19) and (20), respectively. $S(q)$, $\tilde{S}_a(q)$, and $\tilde{S}_a^{-1}(q)$ are taken from the simulation at $T=0.47$.

Figure 2 and its inset examine to what extent the ring approximations (19) and (20) hold for our model. It is seen that, except for $\tilde{S}_1(q)$ and $\tilde{S}_1^{-1}(q)$ referring to the end monomer, the ring approximation is well satisfied, suggesting that this additional approximation can also be used in deriving a theory for polymer dynamics without introducing a large error. Let us add that both the equivalent-site and ring approximations have been found to hold well also for the liquid structure of some semiflexible polymer models [23].

IV. THEORY

A. MCT equations for coherent structural dynamics

In the site formalism, collective structural dynamics are to be described by site-site density correlators

$$F_{ab}(q,t) = \frac{1}{n}\langle \rho_a(\mathbf{q})^* e^{i\mathcal{L}t}\rho_b(\mathbf{q})\rangle \quad (a,b=1,\ldots,N), \quad (21)$$

whose initial values are the static structure factors $S_{ab}(q) = F_{ab}(q,0)$. Here, $\mathcal{L}$ denotes the Liouville operator appropriate for Newtonian dynamics. MCT equations of motion for $F_{ab}(q,t)$ for general flexible molecules are derived in Appendix A, and consist of the Zwanzig-Mori exact equation of motion and an approximate expression for the memory kernel. The former is obtained by introducing a projection operator $\mathcal{P}$ onto the monomer-density fluctuations and the corresponding longitudinal current fluctuations, and reads [see Eq. (A6)]

$$\partial_t^2 F_{ab}(q,t) + \sum_{x=1}^{N} \Omega_{ax}^2(q) F_{xb}(q,t) + \sum_{x=1}^{N} \int_0^t dt' M_{ax}(q,t-t')\partial_{t'} F_{xb}(q,t') = 0. \quad (22)$$

Here $\Omega_{ab}^2(q)$ represents the characteristic frequency given by

$$\Omega_{ab}^2(q) = q^2 v^2 S_{ab}^{-1}(q), \quad (23)$$

with $v^2 = k_B T/m$ ($=T$ in the reduced units) denoting the monomer thermal velocity, and a formally exact expression for the memory kernel reads

$$M_{ab}(q,t) = \frac{1}{nv^2}\langle f_a(\mathbf{q})^* \exp(i\mathcal{Q}\mathcal{L}\mathcal{Q}t) f_b(\mathbf{q})\rangle, \quad (24)$$

in terms of the fluctuating random force $f_a(\mathbf{q})$ which evolves with the generator $\mathcal{Q}\mathcal{L}\mathcal{Q}$, where $\mathcal{Q} \equiv 1-\mathcal{P}$. An approximate expression for $f_a(\mathbf{q})$ as derived under the mode-coupling approach in Appendix A is given by [omitting the irrelevant factor $-i$ from Eq. (A21)]

$$f_a(\mathbf{q}) = \frac{\rho v^2}{n}\sum_{\mathbf{k}}\sum_{x=1}^{N} (\hat{\mathbf{q}}\cdot\mathbf{k}) c_{xa}(k)\rho_x(\mathbf{k})\rho_a(\mathbf{p}), \quad (25)$$

in which $\hat{\mathbf{q}} = \mathbf{q}/q$ and $\mathbf{p} = \mathbf{q}-\mathbf{k}$. With the use of the factorization approximation (A13), one finally arrives at the following MCT expression for the kernel [see Eq. (A22)]:

$$M_{ab}(q,t) = \frac{\rho v^2}{(2\pi)^3}\sum_{x,y=1}^{N}\int d\mathbf{k}[(\hat{\mathbf{q}}\cdot\mathbf{k})^2 c_{ax}(k)c_{by}(k)F_{xy}(k,t) \times F_{ab}(p,t) + (\hat{\mathbf{q}}\cdot\mathbf{k}) \times (\hat{\mathbf{q}}\cdot\mathbf{p})c_{ax}(k)c_{by}(p)F_{xb}(k,t)F_{ay}(p,t)]. \quad (26)$$

Equations (22) and (26) provide a set of closed equations for determining site-site coherent density correlators $F_{ab}(q,t)$, provided the static quantities $S_{ab}(q)$ and $c_{ab}(q)$ are known. From a computational point of view, however, it is quite demanding to solve these $N\times N$ matrix equations, since N may become large for polymeric systems [24]. It is at this point where the analysis of the static properties, presented in Ref. [16] and summarized in Sec. III, will help us to develop further approximations.

As mentioned in Sec. III B, the equivalent-site approximation $c_{ab}(q)=c(q)$ is well justified for our model. So, we insert $c_{ab}(q)=c(q)$ in Eq. (25) and obtain

$$f_a(\mathbf{q}) = \frac{\rho v^2}{n}\sum_{\mathbf{k}} (\hat{\mathbf{q}}\cdot\mathbf{k})c(k)\rho_{\mathrm{tot}}(\mathbf{k})\rho_a(\mathbf{p}), \quad (27)$$

where $\rho_{\mathrm{tot}}(\mathbf{k})$ denotes the total monomer density fluctuations introduced in Eq. (9). This expression reveals that the equivalent-site approximation alone does not suffice to simplify the problem: the dependence of $f_a(\mathbf{q})$ on the monomer position remains, and the resulting $M_{ab}(q,t)$ still carries the (a,b) dependence, i.e., it consists of $O(N^2)$ elements. Furthermore, no simplification is yet achieved concerning the frequency matrix (23).

Progress is made if we invoke the second approximation described in Sec. III C. The frequency term (23) can be simplified by the use of the ring approximation (20) to

$$\sum_{a=1}^{N}\Omega_{ab}^2(q) = q^2v^2\sum_{a=1}^{N} S_{ab}^{-1}(q) \approx q^2v^2/S(q) \equiv \Omega^2(q). \quad (28)$$

A corresponding simplification can be introduced for the fluctuating force $f_a(\mathbf{q})$. To this end, we notice that $f_a(\mathbf{q})$ in Eq. (27) originates from interchain interactions represented through the direct correlation function. It is then reasonable to expect that, for long chains, the specific monomer-position dependence in $f_a(\mathbf{q})$ is small, and can be well approximated by an averaged one. (This approximation is exact for rings.) We therefore introduce an approximation

$$f_a(\mathbf{q}) \approx \frac{1}{N}\sum_{a=1}^{N} f_a(\mathbf{q}). \quad (29)$$

This ring approximation replaces the site-specific surroundings of a monomer by an averaged one, and then the fluctuating force is given by

$$f_a(\mathbf{q}) = \frac{\rho v^2}{nN}\sum_{\mathbf{k}} (\hat{\mathbf{q}}\cdot\mathbf{k})c(k)\rho_{\mathrm{tot}}(\mathbf{k})\rho_{\mathrm{tot}}(\mathbf{p}). \quad (30)$$

This leads to an expression for $M_{ab}(q,t)$ (to be summarized below) which now does not depend on the site indices (a,b).

The approximations discussed so far allow us to derive a set of closed MCT equations for the collective total monomer density correlators

$$F(q,t) \equiv \frac{1}{N}\sum_{a,b=1}^{N} F_{ab}(q,t) = \frac{1}{nN}\langle \rho_{\mathrm{tot}}(\mathbf{q})^* e^{i\mathcal{L}t}\rho_{\mathrm{tot}}(\mathbf{q})\rangle, \quad (31)$$

whose initial value is $F(q,0)=S(q)$ [see Eq. (8)]. To this end, we take $(1/N)\Sigma_{a,b}$ of Eq. (22), and then insert the frequency term (28) and the memory kernel with the fluctuating force given in Eq. (30) under the factorization approximation (A13). This gives the following set of MCT equations for the normalized coherent density correlators $\phi(q,t) \equiv F(q,t)/S(q)$:

$$\partial_t^2\phi(q,t) + \Omega^2(q)\phi(q,t) + \Omega^2(q)\int_0^t dt' m(q,t-t')\partial_{t'}\phi(q,t') = 0, \quad (32)$$

$$m(q,t) = \frac{1}{2}\int d\mathbf{k}\; V(\mathbf{q};\mathbf{k},\mathbf{p})\phi(k,t)\phi(p,t). \quad (33)$$

Here $\Omega^2(q)=q^2v^2/S(q)$, and the vertex function reads

$$V(\mathbf{q};\mathbf{k},\mathbf{p}) = \frac{\rho_{\mathrm{m}}}{(2\pi)^3 q^2}S(q)S(k)S(p)\{\hat{\mathbf{q}}\cdot[\mathbf{k}c(k)+\mathbf{p}c(p)]\}^2. \quad (34)$$

One can solve these equations for $\phi(q,t)$ provided the average static quantities $S(q)$ and $c(q)$ are given as input.

Equations (32) and (33) merit some comments. (i) These equations are formally identical to MCT equations for monatomic liquids. Polymer-specific effects, such as local stiffness of the chain backbone or chain length N, enter the relaxation only via the direct correlation function $c(q)$, the structure factor $S(q)$, and the monomer density ρ_{m}. These static equilibrium features fully determine the long-time coherent dynamics of the melt. (ii) Equations (33) and (34) indicate that the memory kernel contains the factor $S(q)S(k)S(p)$. So the slow dynamics upon lowering T should be mainly driven by wave vectors close to q^* because there, $S(q)$ is largest and the strongest dependence on T occurs (see Sec. III B). Thus, our theory predicts that the glassy structural slowing down is connected to the increase of the first peak of $S(q)$, i.e., to the local cage effect.

We finally notice that the so-called regular contribution to the memory kernel [11] is discarded in our theory, and our approximate memory kernel is completely given by the mode-coupling expression. The latter provides the slow contribution relevant for the structural slowing down. The regular contribution is supposed to embody memory effects already present in the normal high-T state of liquids, and accounts for the fast dynamics in the short-time regime. We drop the regular contribution since it does not affect the MCT predictions for the slow-relaxation regime [11,25]. Thus, care has to be taken in comparing theoretical predictions with simulation results, since the theory without the regular contribution does not properly describe the short-time dynamics [26].

B. MCT equations for single-chain dynamics

The basic variable characterizing the dynamics of a single (or tagged) chain is

$$\rho_a^{\mathrm{s}}(\mathbf{q},t) = e^{i\mathbf{q}\cdot\mathbf{r}_{\mathrm{s}}^a(t)}, \quad (35)$$

where $\mathbf{r}_{\mathrm{s}}^a(t)$ denotes the position of the ath monomer in the tagged (labeled s) chain at time t. The density correlator for the single-chain dynamics is defined by

$$F_{ab}^{\mathrm{s}}(q,t) = \langle \rho_a^{\mathrm{s}}(\mathbf{q})^*\rho_b^{\mathrm{s}}(\mathbf{q},t)\rangle, \quad (36)$$

whose initial value is the intrachain structure factor $w_{ab}(q) = F_{ab}^{\mathrm{s}}(q,0)$.

The derivation of the MCT equations for $F_{ab}^{\mathrm{s}}(q,t)$ is outlined in Appendix A 3, and the resulting matrix equations can be summarized as

$$\partial_t^2 F_{ab}^{\mathrm{s}}(q,t) + \sum_{x=1}^{N}\Omega_{ax}^{\mathrm{s}2}(q)F_{xb}^{\mathrm{s}}(q,t) + \sum_{x,y=1}^{N}\Omega_{ax}^{\mathrm{s}2}(q)\int_0^t dt' m_{xy}^{\mathrm{s}} \times(q,t-t')\partial_{t'}F_{yb}^{\mathrm{s}}(q,t') = 0, \quad (37)$$

where the frequency matrix is given by

$$\Omega_{ab}^{\mathrm{s}2}(q) = q^2v^2w_{ab}^{-1}(q), \quad (38)$$

and the MCT expression for $m_{ab}^{\mathrm{s}}(q,t)$ under the equivalent-site approximation (15) reads

$$m_{ab}^{\mathrm{s}}(q,t) = \sum_{x=1}^{N} w_{ax}(q)\int d\mathbf{k}\; V^{\mathrm{s}}(\mathbf{q};\mathbf{k},\mathbf{p})F_{xb}^{\mathrm{s}}(k,t)\phi(p,t), \quad (39)$$

with the vertex function

$$V^{\mathrm{s}}(\mathbf{q};\mathbf{k},\mathbf{p}) = \frac{\rho_{\mathrm{m}}}{(2\pi)^3 q^2}S(p)(\hat{\mathbf{q}}\cdot\mathbf{p})^2c(p)^2. \quad (40)$$

Equations (37) and (39) constitute a set of closed $(N\times N)$-matrix MCT equations for the single-chain density correlators $F_{ab}^{\mathrm{s}}(q,t)$. One can solve these equations with knowledge of the static quantities—$S(q)$, $c(q)$, and $w_{ab}(q)$—and of the coherent density correlators $\phi(q,t)$. It is clear from Eq. (39) that the slowing down of the single-chain dynamics is driven by that of the coherent dynamics.

Unlike the MCT equations for the coherent dynamics, one cannot simplify the matrix structure of Eqs. (37)–(39) for the single-chain density correlators $F_{ab}^{\mathrm{s}}(q,t)$ in order to properly describe chain-connectivity effects, taken into account through the intrachain structure factor matrix $w_{ab}(q)$. For example, one needs the site-site $F_{ab}^{\mathrm{s}}(q,t)$ to fully describe the chain conformational dynamics, i.e., all the Rouse-mode correlators introduced below, and has to solve the matrix MCT equations (37) and (39) for this purpose. Let us note in this connection that, from a computational point of view, it is not

so demanding to solve these matrix MCT equations for $F^{s}_{ab}(q,t)$. This is because the most time-consuming part in numerically solving the MCT equations is spent in solving the ones for coherent dynamics [27].

C. MCT equations for Rouse-mode correlators

In this section, the site-density description of the single-chain dynamics will be related to the traditional Rouse description, and we derive the MCT equations for the Rouse-mode correlators. Let us stress that the present rewriting is exact and always possible. The N degrees of freedom of segmental motion are mapped onto N modes labeled by p. If the Rouse model holds, the modes will be statistically independent and the matrix of Rouse-mode correlators introduced below becomes diagonal.

Let us introduce the following $N\times N$ orthogonal matrix P_{ap} ($a=1,2,\ldots,N$ and $p=0,1,\ldots,N-1$):

$$P_{ap}=\begin{cases}\sqrt{\dfrac{1}{N}}, & (p=0),\\ \sqrt{\dfrac{2}{N}}\cos\left(\dfrac{(a-1/2)p\pi}{N}\right), & (p=1,2,\ldots,N-1).\end{cases} \tag{41}$$

The Rouse-mode vectors will be defined in terms of the monomer positions as $\mathbf{X}_p(t)=\Sigma_{a=1}^{N}P_{ap}\mathbf{r}^a_s(t)$ [28], i.e.,

$$\mathbf{X}_p(t)=\begin{cases}\sqrt{\dfrac{1}{N}}\displaystyle\sum_{a=1}^{N}\mathbf{r}^a_s(t), & (p=0),\\ \sqrt{\dfrac{2}{N}}\displaystyle\sum_{a=1}^{N}\mathbf{r}^a_s(t)\cos\left(\dfrac{(a-1/2)p\pi}{N}\right), & (p=1,2,\ldots,N-1).\end{cases} \tag{42}$$

The inverse relation is given by $\mathbf{r}^a_s(t)=\Sigma_{p=0}^{N-1}P_{ap}\mathbf{X}_p(t)$:

$$\mathbf{r}^a_s(t)=\sqrt{\frac{1}{N}}\left[\mathbf{X}_0(t)+\sqrt{2}\sum_{p=1}^{N-1}\mathbf{X}_p(t)\cos\left(\frac{(a-1/2)p\pi}{N}\right)\right]. \tag{43}$$

We introduce the Rouse-mode correlators as

$$C_{pp'}(t)=\begin{cases}[\langle\mathbf{X}_0(0)\cdot\mathbf{X}_0(t)\rangle-\langle\mathbf{X}_0(0)\cdot\mathbf{X}_0(0)\rangle]/3N, & (p=p'=0),\\ [\langle\mathbf{X}_0(0)\cdot\mathbf{X}_{p'}(t)\rangle-\langle\mathbf{X}_0(0)\cdot\mathbf{X}_{p'}(0)\rangle]/3N, & (p=0,p'\neq 0),\\ \langle\mathbf{X}_p(0)\cdot\mathbf{X}_{p'}(t)\rangle/3N, & (p\neq 0,p'\neq 0).\end{cases} \tag{44}$$

From the definition, it is obvious that

$$C_{00}(0)=0,\quad C_{0p}(0)=0\quad \text{for } p>0. \tag{45}$$

Let us introduce the following $(N-1)\times(N-1)$ matrix to denote the initial values of $C_{pp'}(t)$ for $p,p'>0$:

$$\hat{C}_{pp'}\equiv C_{pp'}(0)\quad \text{defined only for } p,p'>0. \tag{46}$$

It is necessary to introduce this new matrix in order to discuss the inverse matrix of $C_{pp'}(0)$: the inverse of the $N\times N$ matrix $C_{pp'}(0)$ does not exist because of Eq. (45), whereas that of the $(N-1)\times(N-1)$ matrix $\hat{C}_{pp'}$ does exist, and will be denoted as $\hat{C}^{-1}_{pp'}$.

Since $\mathbf{X}_0(t)=\sqrt{N}\mathbf{R}_s(t)$ with $\mathbf{R}_s(t)$ denoting the c.m. position of the tagged chain at time t, $C_{00}(t)$ is related to the c.m. mean-square displacement (MSD) $g_C(t)=\langle[\mathbf{R}_s(t)-\mathbf{R}_s(0)]^2\rangle$:

$$g_C(t)=-6C_{00}(t). \tag{47}$$

For the monomer MSD $g_a(t)=\langle[\mathbf{r}^a_s(t)-\mathbf{r}^a_s(0)]^2\rangle$, it follows from Eqs. (43) and (44) that

$$g_a(t)=g_C(t)-12\sqrt{2}\sum_{p'=1}^{N-1}C_{0p'}(t)\cos\left(\frac{(a-1/2)p'\pi}{N}\right)+12\sum_{p=1}^{N-1}\sum_{p'=1}^{N-1}[C_{pp'}(0)-C_{pp'}(t)]\times\cos\left(\frac{(a-1/2)p\pi}{N}\right)\cos\left(\frac{(a-1/2)p'\pi}{N}\right). \tag{48}$$

In particular, one gets for the MSD averaged over all the monomers in a chain

$$g_M(t)\equiv(1/N)\sum_{a=1}^{N}g_a(t)=g_C(t)+6\sum_{p=1}^{N-1}[C_{pp}(0)-C_{pp}(t)]. \tag{49}$$

We next consider how the Rouse-mode correlators $C_{pp'}(t)$ are related to the site-density correlators $F^{s}_{ab}(q,t)$. This will allow us to write down MCT equations for the former based on the ones for the latter. Since the density fluctuations of the

tagged chain for small $\mathbf{q}$ are given by $\rho_a^s(\mathbf{q},t) \approx 1 + i\mathbf{q}\cdot\mathbf{r}_s^a(t)$, it is easily understood that $C_{pp'}(t)$ can be expressed as a linear combination of $F_{ab}^s(q,t)$ for $q \to 0$. Indeed, one can show that

$$\frac{1}{N}\sum_{a,b=1}^{N} P_{ap}F_{ab}^s(q\to 0,t)P_{bp'} = \begin{cases} 1 + q^2[C_{00}(t) - A] + O(q^4), & (p = p' = 0), \\ q^2[C_{0p'}(t) - B_{p'}] + O(q^4), & (p = 0, p' > 0), \\ q^2 C_{pp'}(t) + O(q^4), & (p, p' > 0), \end{cases} \tag{50}$$

where $A = (1/6N^2)\Sigma_{a,b=1}^N \langle (\mathbf{r}_s^a - \mathbf{r}_s^b)^2 \rangle = R_g^2/3$ with R_g denoting the radius of gyration of a chain, and $B_p = (1/3\sqrt{2}N^2)\Sigma_{a,b=1}^N \langle (\mathbf{r}_s^a - \mathbf{r}_s^b)^2 \rangle \cos[(b-1/2)p\pi/N]$. Using these relations, one derives the following MCT equations for $C_{pp'}(t)$ by taking the $q \to 0$ limit of Eqs. (37)–(40):

$$\partial_t^2 C_{pp'}(t) + v^2 D_{pp'} + v^2 \sum_{p''=0}^{N-1} E_{pp''}C_{p''p'}(t) + v^2 \sum_{p''=0}^{N-1} \int_0^t dt' m_{pp''}(t-t')\partial_{t'}C_{p''p'}(t') = 0, \tag{51}$$

where

$$D_{pp'} = \delta_{p0}\delta_{p'0}/N, \tag{52}$$

$$E_{pp'} = \begin{cases} \hat{C}_{pp'}^{-1}/N, & (p, p' > 0), \\ 0 & \text{otherwise}. \end{cases} \tag{53}$$

and the expression for the memory kernel reads

$$m_{pp'}(t) = \frac{\rho_m}{6\pi^2}\int dk\, k^4 S(k) c(k)^2 \left(\sum_{a,b=1}^{N} P_{ap}F_{ab}^s(k,t)P_{bp'} \right) \phi(k,t). \tag{54}$$

These MCT equations for $C_{pp'}(t)$ can be solved provided the static quantities—$S(q)$, $c(q)$, $w_{ab}(q)$, and $\hat{C}_{pp'}$—and the full site-site single-chain density correlators $F_{ab}^s(q,t)$ as well as the coherent density correlators $\phi(q,t)$ are known. MSDs can then be obtained from Eqs. (47)–(49). Again, it is clear from Eq. (54) that the slowing down of the Rouse-mode dynamics and MSDs is dictated by that of the coherent dynamics. In Appendix B, we will show how the Rouse model emerges from our MCT equations in the asymptotic limit of large N.

D. Universal MCT predictions

Here, we briefly summarize some universal MCT predictions which are necessary for understanding the present paper. As described in Ref. [29], all universal results concerning the MCT-liquid-glass transition dynamics, originally developed for simple systems [11], are also valid for molecular systems, and the MCT for polymer melts developed in Sec. IV shares this feature. This justifies the use of the MCT universal predictions in analyzing polymer data, whose validity has been tacitly assumed in previous studies of our model [4,8,30].

One of the central predictions of MCT is the existence of a critical temperature T_c. The long-time limit, or the nonergodicity parameter, of the coherent density correlator $f(q) \equiv \phi(q, t\to\infty)$ obeys the implicit equation

$$\frac{f(q)}{1-f(q)} = \mathcal{F}_q[f], \tag{55}$$

which can be derived by taking the $t \to \infty$ limit of Eqs. (32) and (33) and introducing the mode-coupling functional $\mathcal{F}_q[f] \equiv (1/2)\int d\mathbf{k}\, V(\mathbf{q};\mathbf{k},\mathbf{p}) f(k) f(p)$. One gets trivial solutions $f(q) = 0$ for $T > T_c$, meaning that the density fluctuations relax completely at long times, a characteristic feature of the ergodic liquid state. On the other hand, nontrivial solutions $f(q) > 0$ can be obtained for $T \le T_c$, describing nonergodic dynamics in which density fluctuations cannot fully decay. The nonergodicity parameter $f(q)$ measures the "solidity" of such an amorphous solid on length scales $\approx 2\pi/q$, and is thus also referred to as the glass form factor or the Debye-Waller factor. The ergodic-to-nonergodic transition at T_c is called the idealized glass transition, and $f(q)$ at $T = T_c$, to be denoted as $f^c(q)$, is referred to as the critical nonergodicity parameter. It also has the meaning of the plateau height in the two-step relaxation of $\phi(q,t)$, and quantifies the strength of its α relaxation (see below).

MCT predicts that for temperatures close to but above T_c, to which we restrict our attention in the following, the dynamics of any time-dependent correlation function $\phi_X(t)$ coupling to density fluctuations exhibits a two-step relaxation: the relaxation toward the plateau, and the final relaxation from the plateau to zero. These relaxations are respectively characterized by the time scales t_σ and t'_σ defined by

$$t_\sigma = t_0/|\sigma|^\delta, \quad \delta = 1/2a, \tag{56}$$

$$t'_\sigma = t_0 B^{-1/b}/|\sigma|^\gamma, \quad \gamma = (1/2a) + (1/2b). \tag{57}$$

Here t_0 denotes some microscopic time scale [31]. σ is called the separation parameter, and measures the distance from the critical point:

$$\sigma = C\varepsilon, \quad \varepsilon = (T_c - T)/T_c. \tag{58}$$

Except for t_0, all the exponents and the constants B and C appearing in these equations can be evaluated from the mode-coupling functional $\mathcal{F}_q[f]$ with the knowledge of $f^c(q)$ [11,32]. According to MCT, the dynamics dramatically slows down upon lowering T since the time scales t_σ and t'_σ diverge for $T \to T_c+$. The two-step-relaxation scenario emerges since the T dependence of t'_σ is stronger than that of t_σ.

The dynamics that occurs near the plateau is referred to as the β process. The height of the plateau is given by the critical nonergodicity parameter f_X^c of the correlator $\phi_X(t)$, which can be determined from the corresponding mode-coupling functional via an equation analogous to Eq. (55).

MCT predicts that there holds for $\sigma \to -0$ (i.e., for $T \to T_c+$)

$$\phi_X(t) = f_X^c + h_X \sqrt{|\sigma|} g(t/t_\sigma) + O(\sigma). \tag{59}$$

Here h_X is called the critical amplitude and $g(\hat{t})$ the β correlator [11]. Equation (59) is called the factorization theorem, according to which the dependence of the correlator $\phi_X(t)$ on X (e.g., the wave number) represented through h_X is factored from the temperature and time dependence described by $\sqrt{|\sigma|} g(t/t_\sigma)$.

The decay of $\phi_X(t)$ down from the plateau f_X^c is called the α process. For this process, MCT predicts for $\sigma \to -0$

$$\phi_X(t) = \tilde{\phi}_X(t/t'_\sigma), \tag{60}$$

which is also referred to as the superposition principle. The temperature-independent shape function $\tilde{\phi}_X(\tilde{t})$—referred to as the α master function—is to be evaluated from the MCT equations at $T=T_c$, and the temperature dependence is given via the time scale t'_σ introduced in Eq. (57). The initial part of the α process is given by the von Schweidler law $\phi_X(t)=f_X^c - h_X(t/t'_\sigma)^b$ [11]. The superposition principle implies that the α relaxation time τ_X of any dynamical variable, defined, e.g., via the convention $\phi_X(\tau_X)=0.1$ which will be employed in this paper, is proportional to t'_σ, i.e.,

$$\tau_X = C_X t'_\sigma. \tag{61}$$

This implies that the unspecified microscopic time scale t_0, which is common to all dynamical quantities, can be eliminated by choosing a particular variable X, e.g., the collective density correlator $\phi(q,t)$ at the structure factor peak position q^*, and then plotting other quantities as a function of t/τ_{q^*} where τ_{q^*} denotes the α relaxation time of $\phi(q^*,t)$.

For our model, the mentioned MCT universal predictions have been successfully applied to analyze simulation data, from which various characteristic quantities have been extracted [4,8,30]. For example, the critical temperature $T_c^{MD} \approx 0.45$ was obtained from the consistent analysis of both β and α relaxations. Critical nonergodicity parameters have been determined for several correlators by applying Eq. (59), including its leading correction [32], in the β regime. These simulation results can directly be compared with our first-principles theoretical calculations.

In addition, and more importantly, our microscopic theory developed here can make predictions concerning polymer-specific features which are outside the scope of the universal MCT predictions. Through the comparative study of such first-principles theoretical predictions and simulation results, we will propose an atomistic interpretation of the slow structural and conformational dynamics of supercooled polymer melts.

V. RESULTS AND DISCUSSION

A. Collective structural dynamics

We start by comparing theoretical and simulation results for the critical glass form factors $f^c(q)$ of the coherent density correlators $\phi(q,t)$. The theoretical result for $f^c(q)$ can be obtained by solving Eq. (55) provided static inputs at T_c^{MCT} are known. [T_c determined from the theory based on the analysis of Eq. (55) will be denoted as T_c^{MCT} to discriminate it from T_c^{MD} obtained from previous analyses [4,8] of the simulation data.] If T_c^{MCT} lies in the range of temperatures for which simulation results are available, the static inputs at T_c^{MCT} can be determined accurately. However, a problem arises if T_c^{MCT} is found to be below the lowest simulated T. This was the case in our study. (See Sec. VI for a possible explanation.) So we had to estimate the required static input by a linear extrapolation based on the simulated $S(q)$ at $T=0.47$ and 0.48. (No extrapolation was necessary for static intrachain correlation functions since they are nearly independent of T as shown in Ref. [16]) The dashed line in Fig. 3(a) shows the extrapolated $S(q)$ at $T_c^{MCT} \approx 0.277$ ($< T_c^{MD} \approx 0.45$) and the inset compares its behavior close to the first-peak position q^* with the simulated $S(q)$ at $T=0.47$, 0.48, and 1. For the simulated $S(q)$ the peak height increases and the peak position shifts to larger q upon lowering T as discussed in Sec. III A. The extrapolated $S(q)$ inherits this trend. This suggests that the physics should not be significantly altered due to possible errors in our extrapolation.

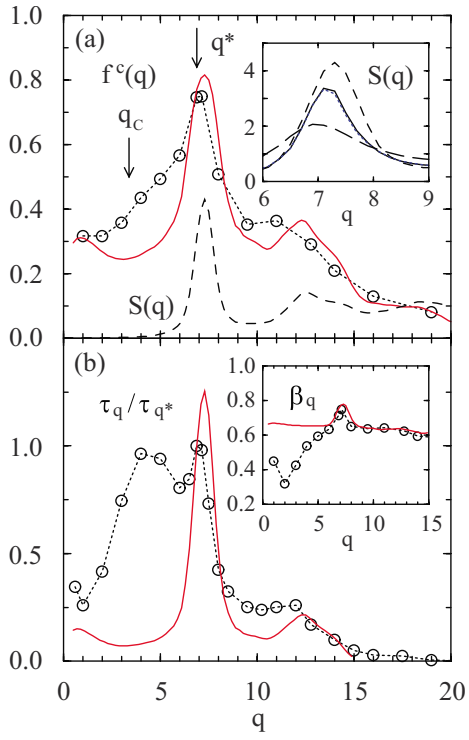

FIG. 3. (Color online) (a) Glass form factors $f^c(q)$ of the coherent density correlators $\phi(q,t)$ versus q. The circles represent the result from the simulation at $T=0.47$, and the solid line that from MCT. The dashed line denotes the extrapolated $S(q)$ (multiplied by 0.1) at $T_c^{MCT} \approx 0.277$. The arrows indicate the peak positions q^* and q_C of $S(q)$ and $S_C(q)$ (see Fig. 1). The inset depicts the extrapolated $S(q)$ at T_c^{MCT} (dashed line), and the simulated $S(q)$ at $T=0.47$ (solid line), 0.48 (dotted line), and 1 (long-dashed line) around the peak q^*. (b) Rescaled α relaxation times τ_q/τ_{q^*} (main panel) and the stretching exponent β_q (inset) of $\phi(q,t)$ versus q. The circles represent the result from the simulation at $T=0.47$, and the solid line that from MCT.

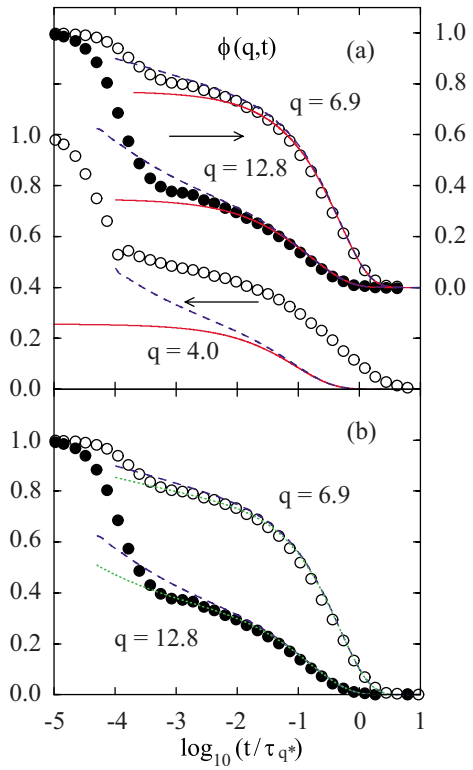

FIG. 4. (Color online) (a) $\phi(q,t)$ as a function of t/τ_{q^*} for $q=4.0$ (left scale), 6.9 (right scale), and 12.8 (right scale). τ_{q^*} is the α relaxation time at q^*. The circles refer to the simulation results at $T=0.47$, the solid lines to the MCT α master curves, and the dashed lines to the MCT curves at the distance parameter $\varepsilon^{\mathrm{MCT}}=-0.046$. (b) $\phi(q,t)$ as a function of t/τ_{q^*} for $q=6.9$ and 12.8. The circles and the dashed lines are the same as in (a), but here the dotted lines denoting the MCT curves at the distance parameter $\varepsilon^{\mathrm{MCT}}=-0.022$ are included as well.

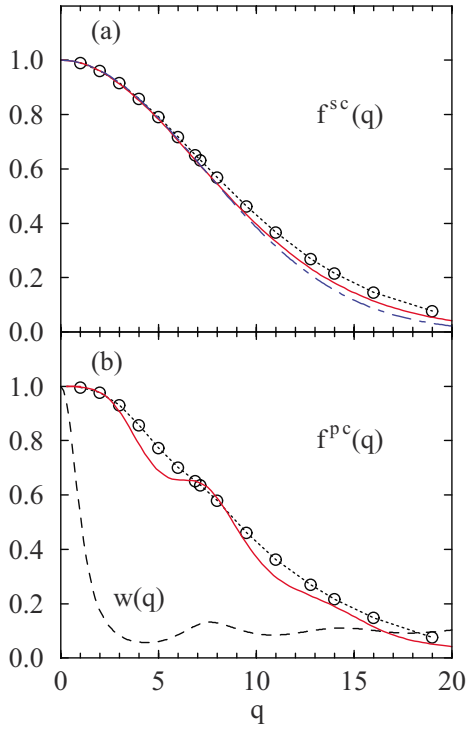

FIG. 5. (Color online) Glass form factors $f^{\mathrm{sc}}(q)$ of the correlators $\phi^{\mathrm{s}}(q,t)$ (a) and $f^{\mathrm{pc}}(q)$ of the correlators $\phi^{\mathrm{p}}(q,t)$ (b) as functions of the wave number q. The circles represent the result from the simulation at $T=0.47$, and the solid line that from MCT. The dash-dotted line in (a) denotes $f_{\mathrm{G}}^{\mathrm{sc}}(q)$ based on the Gaussian approximation (64) with the value $r_{\mathrm{M}}^{\mathrm{c}}=0.098$ taken from the theoretical calculation. The dashed line in (b) shows the simulated $w(q)$ (multiplied by 0.1) at $T=0.47$.

Figure 3(a) compares $f^{\mathrm{c}}(q)$ from MCT with the simulation result determined in Ref. [4]. For $q\gtrsim q^*=6.9$, i.e., for distances comparable to the average monomer separation, we find a high degree of accord between theory and simulation. In particular, the agreement is quite good at q^*, which is gratifying since the coherent dynamics for wave vectors close to q^* drives the glassy slowing-down [see the second comment below Eq. (34)]. On the other hand, the theory fails to reproduce the shoulder present in the simulation results at intermediate q near the peak $q_{\mathrm{C}}=3.4$ of $S_{\mathrm{C}}(q)$.

A similar conclusion can be drawn for the α relaxation time τ_q, defined via the convention $\phi(q,\tau_q)=0.1$, which is shown in Fig. 3(b). τ_q depends nonmonotonically on q and varies over an order of magnitude from $\tau_{q^*}\approx 1500$ to $\tau_{q=16}\approx 40$ [4]. The theory semiquantitatively captures these trends for $q\gtrsim q^*$, but misses the peak around q_{C}. We also find corresponding deviations at $q\approx q_{\mathrm{C}}$ in the relaxation stretching, as demonstrated in the inset of Fig. 3(b), quantified in terms of the stretching exponent β_q, which is obtained via a Kohlrausch-law fit of the α-decay part of the correlator, $\phi(q,t)\propto\exp[-(t/\tau_q')^{\beta_q}]$.

The circles in Fig. 4(a) show $\phi(q,t)$ for $q=4.0$, 6.9, and 12.8, obtained from simulations at $T=0.47$, which is close to $T_{\mathrm{c}}^{\mathrm{MD}}\approx 0.45$. Clear evidence for the presence of a two-step relaxation exists. As described in Sec. IV D, MCT provides, up to a time scale t_0 common to all dynamical quantities, quantitative predictions for the α regime in terms of the (T-independent) α master curves, which are drawn as solid lines in Fig. 4(a). The dynamics including the early β regime can be described by solving the MCT equations for a temperature T above $T_{\mathrm{c}}^{\mathrm{MCT}}$, which will be characterized by the distance parameter $\varepsilon^{\mathrm{MCT}}=(T_{\mathrm{c}}^{\mathrm{MCT}}-T)/T_{\mathrm{c}}^{\mathrm{MCT}}$. The dashed curves in Fig. 4(a) present such theoretical results for $\varepsilon^{\mathrm{MCT}}=-0.046$, which corresponds to the distance between $T=0.47$ and $T_{\mathrm{c}}^{\mathrm{MD}}\approx 0.45$ of the simulation results. Since the separation parameter controls the ratio of the time scales characterizing the β and α relaxation regimes [see Eqs. (56) and (57)], we found that a better agreement in the early β regime can be achieved by treating $\varepsilon^{\mathrm{MCT}}$ as a fit parameter. The theoretical results for $\varepsilon^{\mathrm{MCT}}=-0.022$, which was chosen so as to reproduce better the time-scale ratio found in the simulation data, are shown as dotted lines in Fig. 4(b). All the theoretical and simulation curves shown in Figs. 4(a) and 4(b) are plotted versus t/τ_{q^*}, with τ_{q^*} being the α relaxation time at q^*. In this way, the unspecified time scale t_0 can be eliminated [see the discussion below Eq. (61)], and the theoretical prediction for the q dependence of the α relaxation times can be examined.

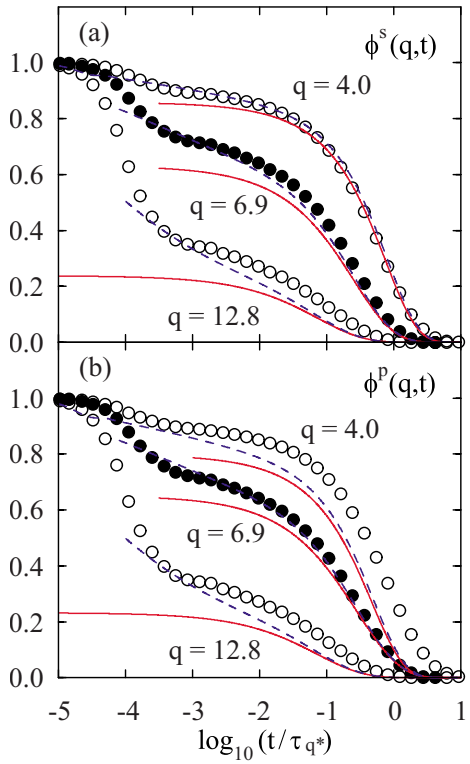

FIG. 6. (Color online) Single-chain density correlators $\phi^s(q,t)$ (a) and $\phi^p(q,t)$ (b) as functions of t/τ_{q^*} for $q=4.0$, 6.9, and 12.8. τ_{q^*} is the α relaxation time of the coherent density correlator $\phi(q,t)$ at $q=q^*$. The circles refer to the simulation results at $T=0.47$, the solid lines to the MCT α master curves, and the dashed lines to the MCT curves at the distance parameter $\varepsilon^{\mathrm{MCT}}=-0.046$.

Figures 4(a) and 4(b) demonstrate that, for $q=6.9$ and 12.8, the MCT curves quantitatively describe the simulation results in both the β and α regimes, including the relative magnitude of τ_q and the stretching of the relaxation. (The disagreement for short times arises mainly because, as mentioned at the end of Sec. IV A, the regular part of the memory kernel is not included in our theory.) On the other hand, the agreement is not satisfactory at $q\approx q_C$. We thus conclude from Figs. 3 and 4 that, except for a process that occurs at $q\approx q_C$, our theory describes the coherent structural dynamics of polymer melts at a semiquantitative level. Since, as will be discussed at the end of Sec. V D, the dynamics at $q\approx q_C$ does not appear to be directly related to the glass transition, this verifies one of the principal predictions of our theory: the emergence of the glassy slow dynamics is connected to the increase of the first peak of $S(q)$, i.e., to the local cage effect. We will further comment on the dynamics at $q\approx q_C$ below.

B. Single-chain density correlators

We next consider the single-chain density correlators. This will be done in terms of the averaged single-segment correlators $\phi^s(q,t)$ and the (normalized) collective single-chain correlators $\phi^p(q,t)$ defined by

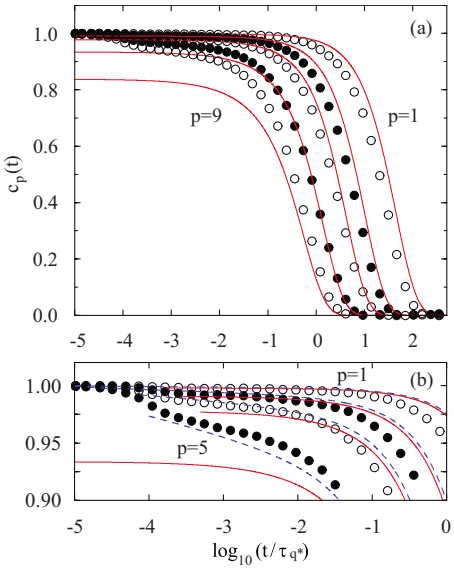

FIG. 7. (Color online) (a) Normalized Rouse-mode correlators $c_p(t)=C_{pp}(t)/C_{pp}(0)$ as a function of t/τ_{q^*} for $p=1$, 2, 3, 5, and 9 (from right to left). τ_{q^*} is the α relaxation time of the coherent density correlator $\phi(q,t)$ at $q=q^*$. The circles refer to the simulation results at $T=0.47$, and the solid lines to the MCT α master curves. (b) Enlargement of the β region in (a); the results for $p=9$ are omitted. Here, dashed lines represent the MCT curves at the distance parameter $\varepsilon^{\mathrm{MCT}}=-0.046$.

$$\phi^s(q,t) = (1/N)\sum_{a=1}^{N} F^s_{aa}(q,t), \tag{62}$$

$$\phi^p(q,t) = (1/N)\sum_{a,b=1}^{N} F^s_{ab}(q,t)/w(q). \tag{63}$$

$\phi^s(q,t)$ is defined solely in terms of the diagonal ($a=b$) elements of $F^s_{ab}(q,t)$, i.e., it probes only the self-motion of monomers, whereas $\phi^p(q,t)$ reflects also interference effects from other monomers belonging to the same chain through the off-diagonal ($a\neq b$) elements. The simulation results for these correlators for our model have been analyzed in Ref. [4].

Theoretical and simulation results for the critical nonergodicity parameters of $\phi^s(q,t)$ and $\phi^p(q,t)$, to be denoted as $f^{sc}(q)$ and $f^{pc}(q)$, are compared in Figs. 5(a) and 5(b). The theoretical results are determined from an equation analogous to Eq. (55), which can be obtained by taking the $t\to\infty$ limit of Eqs. (37) and (39). The full time dependence of the correlators $\phi^s(q,t)$ and $\phi^p(q,t)$ for representative wave numbers are shown in Figs. 6(a) and 6(b), where the MCT α master curves and the MCT curves at the distance parameter $\varepsilon^{\mathrm{MCT}}=-0.046$ are compared with the simulated correlators at $T=0.47$. All the curves in Figs. 6(a) and 6(b) are plotted versus t/τ_{q^*}, with τ_{q^*} being the α relaxation time of the coherent density correlator $\phi(q,t)$ at $q=q^*$. In this way, the theoretical predictions not only for the q dependence of the α relaxation times of $\phi^s(q,t)$ and $\phi^p(q,t)$, but also for the rela-

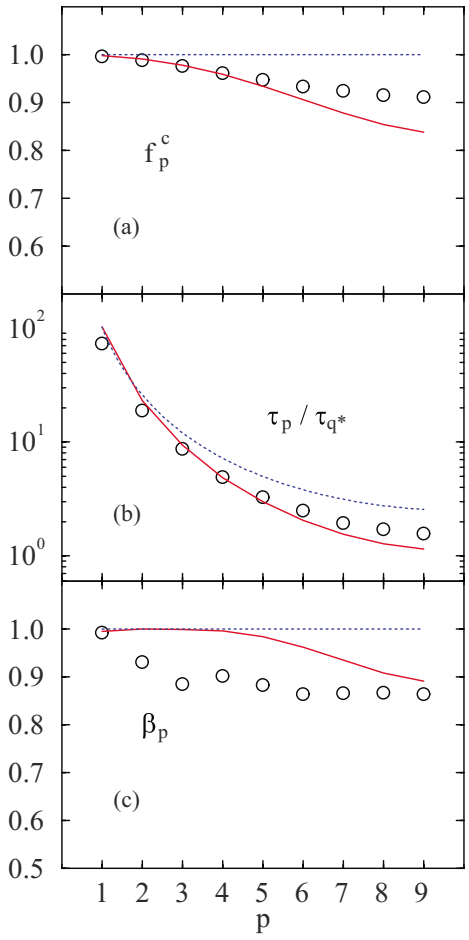

FIG. 8. (Color online) The plateau heights f_p^c (a), the ratio τ_p/τ_{q^*} of the α relaxation times (b), and the stretching exponent β_p (c) of the Rouse-mode correlators $c_p(t)$ as a function of the mode index p. The circles represent the result from the simulation at $T=0.47$, and the solid line that from MCT. The dotted line in each panel refers to pure Rouse behavior predicted by our theory in the asymptotic limit of large N (see Appendix B): $f_p^c=1$, $\tau_p \propto [\sin(p\pi/2N)]^{-2}$, and $\beta_p=1$.

tive time scale of the single-chain and coherent dynamics, can be tested.

We first notice from Fig. 5(a) that the theory (solid line) describes well the simulated $f^{sc}(q)$ (circles) including the wave numbers $q \lesssim q^*$. This appears to be inconsistent with the result for the coherent dynamics, where we found disagreement at $q \approx q_C$, but can be understood in the following way. In the small-q limit, the relation $\phi^s(q \to 0,t)=1-(q^2/6)g_M(t)+O(q^4)$ holds, in terms of the monomer-averaged MSD, which implies the Gaussian approximation $\phi_G^s(q,t) \approx \exp[-(q^2/6)g_M(t)]$. The discussion of $g_M(t)$ will be presented in Sec. V D, but let us mention here that the critical nonergodicity parameter $6(r_M^c)^2$ of $g_M(t)$—the plateau height of $g_M(t)$ in the β regime—quantifies the size of the cage of a monomer formed by its surroundings. Thus, one expects the approximation

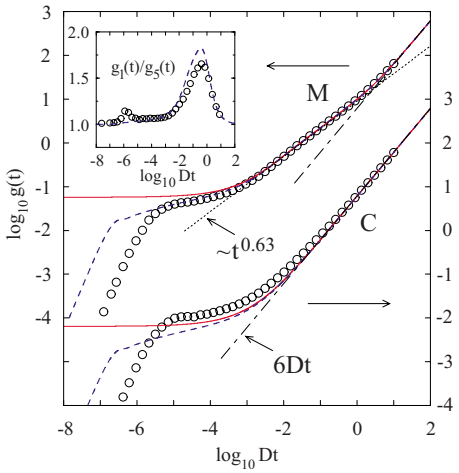

FIG. 9. (Color online) Double-logarithmic presentation of the MSDs $g_M(t)$ (labeled M, left scale) and $g_C(t)$ (labeled C, right scale) as a function of Dt. The inset exhibits the ratio $g_1(t)/g_5(t)$ (end over middle monomer MSD). The circles refer to the simulation results at $T=0.47$, the solid lines to the MCT α master curves, and the dashed lines to the MCT curves at the distance parameter $\epsilon^{MCT}=-0.046$. The dash-dotted lines indicate the diffusion law $6Dt$, while the dotted line shows the power law $\sim t^{0.63}$.

$$f_G^{sc}(q) \approx \exp[-q^2(r_M^c)^2] \tag{64}$$

to be valid at least for small q. The dash-dotted line in Fig. 5(a) shows $f_G^{sc}(q)$ with the value $r_M^c=0.098$ taken from the theoretical calculation. It is seen that $f_G^{sc}(q)$ describes well both the theoretical and simulated $f^{sc}(q)$. This reveals that the q dependence of $f^{sc}(q)$ mostly reflects the spatial extent of the localized monomer motion in the β relaxation regime, and that our theory quantitatively describes the simulated $f^{sc}(q)$, since it correctly predicts the size of the cage. Figure 6(a) furthermore indicates that not only the dynamics in the β-relaxation regime where the correlators $\phi^s(q,t)$ are close to the plateaus $f^{sc}(q)$, but also their α decay, is well described by the theory, including the relative time scale of the single-chain and coherent dynamics.

In contrast to $f^{sc}(q)$, we expect some interference effects due to chain connectivity to be visible in $f^{pc}(q)$ on top of the nearly Gaussian background just mentioned. The theoretical prediction for $f^{pc}(q)$, shown as the solid line in Fig. 5(b), indeed exhibits an oscillatory feature which is in phase with $w(q)$. The oscillatory q variation of $w(q)$ in turn reflects the bonding effect as discussed in Ref. [16]. In the simulated $f^{pc}(q)$, shown as circles in Fig. 5(b), the presence of such oscillations as predicted by the theory is discernible, though its amplitude is much smaller. [The oscillation in the simulated $f^{pc}(q)$, though tiny, can more easily be grasped in Fig. 8 of the first paper in Ref. [4] where both of the simulated $f^{sc}(q)$ and $f^{pc}(q)$ are plotted in one panel.] This explains, e.g., why the theory does not describe so well the simulated $\phi^p(q,t)$ at $q=4.0$ [Fig. 6(b)], in spite of the fact that it well describes the simulated $\phi^s(q,t)$ at the same wave number [Fig. 6(a)]: the oscillatory q dependence of the plateau height

and the α relaxation time is more pronounced in the theoretical prediction.

C. Rouse-mode dynamics

We next turn our attention to the Rouse-mode correlators $C_{pp'}(t)$ describing the chain conformational dynamics. Circles in Fig. 7(a) show the simulation results for the normalized Rouse-mode correlators $c_p(t)=C_{pp}(t)/C_{pp}(0)$ at $T=0.47$ for representative mode indices p. It is seen that $c_p(t)$ do not clearly exhibit the two-step relaxation. This is because the plateaus f_p^c of $c_p(t)$ are so large [$f_p^c \gtrsim 0.9$ for simulation results as shown in Fig. 8(a)] that only about 10% or less of the decay is left for the relaxation towards the plateau. Thus, most of the relaxation of $c_p(t)$ occurs in the α regime. We therefore included for comparison only the MCT α master curves as solid lines in Fig. 7(a), and the comparison including the early β regime is done separately in Fig. 7(b), which highlights the plateau regime. For a more quantitative comparison of the features in the α relaxation, theoretical and simulation results for the plateau heights f_p^c, the α relaxation time τ_p defined via the convention $c_p(\tau_p)=0.1$, and the stretching exponent β_p based on the Kohlrausch-law fit of $c_p(t)$ are compared in Fig. 8 for all the Rouse modes p.

It is seen from Figs. 7 and 8 that our first-principles theory describes at a semiquantitative level the main features of the simulation results for $c_p(t)$, such as the high plateau values f_p^c and the nearly exponential relaxation ($\beta_p \gtrsim 0.9$). In particular, from the comparison of the ratio τ_p/τ_{q^*} of the α relaxation times shown in Fig. 8(b), we see that the theory provides a good description of the time-scale separation of the single-chain conformational fluctuations (characterized by τ_p) from the local dynamics of the surrounding medium (τ_{q^*}), which becomes more pronounced with decreasing p.

The Rouse theory assumes a chain to be in a Markovian heat bath, i.e., that all dynamical correlations in the surroundings are much faster than the single-chain dynamics [2]. However, since a polymer is surrounded by identical polymers, the assumption of the time-scale separation cannot be justified *a priori*. Our microscopic theory developed here verifies this central assumption from first principles: our theory predicts the time-scale separation for small p/N, and hence, the Markovian approximation can be justified for small Rouse-mode indices (see Appendix B). The simulated results for the Rouse-mode correlators do not exhibit pure Rouse behavior due to finite-N effects (see Appendix B 4), and even such deviations can be semiquantitatively accounted for by our theory, as demonstrated in Fig. 8 where the pure Rouse behavior is also included for comparison.

On the other hand, we also observe features predicted by the Rouse model, in both the simulated and theoretical results, already for such short chains as $N=10$. Let us recall from Ref. [33] that the matrix of the equilibrium values of the (unnormalized) Rouse-mode correlators for our model is close to diagonal, $C_{pp'}(t=0) \sim \delta_{pp'}$, and that the amplitude $C_{pp}(t=0)$ for the smallest p is approximately given by the Gaussian result. It is an important numerical observation within our approach that the Rouse-mode correlators $C_{pp'}(t)$ remain nearly diagonal for all the times, in agreement with the simulation result, and that the time-scale separation holds rather well between the memory functions in Eq. (54) and the Rouse-mode correlators for the smallest p. This holds because collective density fluctuations at microscopic wavelengths dominate the memory functions. This is also the reason why the theory yields asymptotically the Rouse model spectrum in the large-N limit and the characteristic $\sqrt{t}$ anomaly in the average segmental MSD (see Appendix B).

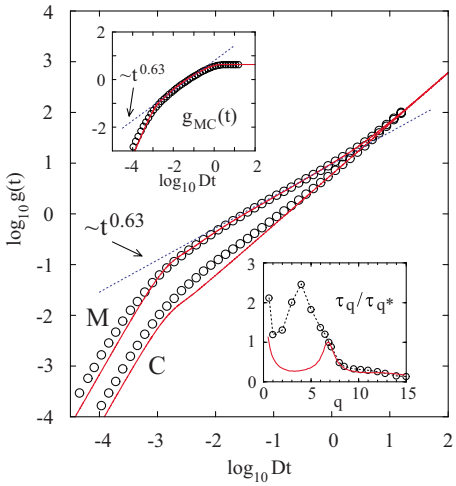

FIG. 10. (Color online) Double-logarithmic presentation of $g_M(t)$ (labeled M) and $g_C(t)$ (labeled C) versus Dt at $T=1$. The upper inset exhibits $g_{MC}(t) \equiv g_M(t) - g_C(t)$, whereas the lower inset shows the q dependence of the ratio τ_q/τ_{q^*} of the α relaxation times of the coherent density correlators $\phi(q,t)$ at $T=1$. The circles represent the result from the simulation, and the solid line that from MCT. The dotted line in the main panel and the upper inset denotes the power law $\sim t^{0.63}$.

D. Mean-square displacements

Now, let us see how the Rouse-mode dynamics affects the single-chain diffusional processes. The circles in Fig. 9 show the simulation results for the monomer-averaged MSD $g_M(t)$ and the c.m. MSD $g_C(t)$. The MSDs also exhibit a two-step relaxation: after the short-time ballistic regime $g_X(t) \propto t^2$ (X=M or C), the increase of the MSD begins to be suppressed due to the cage effect, and there appears the β regime where $g_X(t)$ is close to a plateau which will be denoted as $6(r_X^c)^2$. The appearance of the plateau regime reflects the confined dynamics of monomers inside the cage, and the height of the plateau of the monomer MSD $g_M(t)$ reflects the size of the cage. We find both from theory and simulation $r_M^c \approx 0.1$ (see Fig. 9), i.e., the amplitude of the confined dynamics inside the cage is about 10% of the monomer diameter. The increase of $g_X(t)$ above the plateau toward the diffusion asymptote, $g_X(t)=6Dt$ with D denoting the diffusion constant, is the α process of the MSD. In contrast to $g_C(t)$, $g_M(t)$ in this regime is significantly affected by chain connectivity since the monomers participate in the conformational motion and most of the conformational fluctuations reflected by $c_p(t)$ occur in the α regime as mentioned above. As a result, a polymer-specific anomaly in the MSD—a subdiffusive

($\sim t^x$) regime—emerges in $g_M(t)$ in the α regime. Since MCT predicts the presence of the von Schweidler–law process as a universal feature (see Sec. IV D), such a polymer-specific feature shows up after the end of the von Schweidler–law process but before the onset of final diffusion [15].

In Fig. 9 the data are plotted versus Dt so that the simulated and theoretical curves coincide in the diffusive late-α regime. This representation facilitates the comparison in the β and early-α regimes. (Plotting MSDs versus t/τ_{q^*} as in Figs. 4 and 7 leads to a horizontal shift of the theoretical curves to the right by a factor of about 0.3 on the $\log_{10} t$ axis.) Figure 9 demonstrates that the theory in terms of the MCT α master curve (solid line) describes the polymer-specific subdiffusive variation of the α process, where $g_M(t) \sim t^x$ with $x=0.63$. Solving the MCT equations for $\varepsilon^{MCT}=-0.046$, whose results are drawn as dashed lines in Fig. 9, the description of the simulated $g_M(t)$ can be extended to about seven decades in t. Our theory derives the Rouse result $x=1/2$ for $N\to\infty$ (see Appendix B and Ref. [15]), in agreement with simulations of long chains in which topological constraints are eliminated [34]. Thus, we suggest that the somewhat larger $x=0.63$ found in our $N=10$ model is a deviation from the pure Rouse behavior due to finite-N effects (see Appendix B 4).

The inset of Fig. 9 compares the ratio $g_1(t)/g_5(t)$ of the MSDs for the end $[g_1(t)]$ and central $[g_5(t)]$ monomers in a chain. This ratio is 1 in the ballistic and diffusive regimes, and exhibits a maximum for times where conformational motion dominates the dynamics [i.e., for t where $g_M(t) \sim t^{0.63}$]. The ratio is also close to 1 in the β regime, indicating that the cage effect slows the motion of end and inner monomers in the same way. This is because the dynamics in the β regime is dominated by the confined dynamics of the monomers inside the cage. The inset of Fig. 9 also reveals semiquantitative agreement between theory and simulation for later times where the ratio exhibits a maximum. This indicates that the motion of the end monomer and that of the central monomer are well discriminated by the theory. Thus, chain-end effects for the dynamics of a tagged chain are properly taken into account by our theory, even though this effect was neglected in the (static) direct correlation functions [see Eq. (15)]. This is because the matrix structure of Eqs. (37) and (39) is preserved for describing the single-chain dynamics. The found agreement of the ratio $g_1(t)/g_5(t)$ also shows that its maximum value, which is somewhat smaller than 2—the result expected from the Rouse theory—reflects deviations due to finite-N effects.

Concerning $g_C(t)$, on the other hand, the theory is not so satisfactory: besides the underestimated plateau height, a careful examination of Fig. 9 indicates that the theoretical $g_C(t)$ enters the diffusion regime earlier than the simulated one. We will come back to this point in the following. We only notice here that the disagreement in $g_C(t)$ does not carry over to $g_M(t)$, because $g_M(t) \gg g_C(t)$ for times before the onset of the final diffusion regime.

As discussed above, our theory yields a subdiffusive, Rouse-like behavior close to T_c. Clearly, this polymer-specific feature is also present in the simulation at high T. However, as T increases, the cage effect loses its importance, and it is thus not clear *a priori* to what extent the theory can still be applied. To examine this, we analyze in Fig. 10 the MSDs at $T=1$, which is more than twice T_c^{MD}. Here, the theory utilizes $S(q)$ taken directly from the simulation at this temperature. Figure 10 indicates that, beyond the short-time regime, the agreement between theory and simulation is very good for $g_M(t)$. In particular, we find $g_M(t) \sim t^{0.63}$ with the same exponent. Thus, though originally developed to describe glassy dynamics, our theory can also properly deal with the conformational dynamics in normal liquid states.

The upper inset of Fig. 10 exhibits the function $g_{MC}(t) \equiv g_M(t) - g_C(t)$. According to Eq. (49), this function highlights the contributions from the chain conformational fluctuations to $g_M(t)$, and depends only on the Rouse modes of nonzero mode indices $p>1$. The inset clearly indicates that the subdiffusive behavior $\sim t^{0.63}$ entirely comes from the Rouse modes, and that the exponent 0.63 does not reflect a crossover effect from the pure Rouse behavior to the final diffusion (i.e., $At^{0.5}+6Dt \nsim t^{0.63}$), but is indeed due to finite-N effects.

On the other hand, we find at $T=1$ again the same disagreement for $g_C(t)$ and for the ratio τ_q/τ_{q^*}. (i) The theoretical $g_C(t)$ enters the diffusion regime earlier than the simulated one which additionally exhibits a subdiffusive behavior $g_C(t) \sim t^y$ with $y \approx 0.8$, known as "anomalous c.m. diffusion" [7,35]. (ii) The theoretical α relaxation times τ_q of $\phi(q,t)$ agree quantitatively with the simulation for $q \gtrsim q^*$, but not for $q \approx q_C$ (see the lower inset of Fig. 10). Thus, the disagreements observed at $T=0.47$ are already present at high T, suggesting that they are not directly related to the glass transition.

VI. SUMMARY AND CONCLUDING REMARKS

In this paper, we proposed a unified first-principles description of the collective structural slowing down and of the single-chain conformational fluctuations in a melt of unentangled polymers. The description requires static input which can be taken directly from simulations, uses approximations like the equivalent-site approximation that can be tested explicitly [16], and attains semiquantitative agreement with simulation results concerning collective as well as single-chain dynamics. Our comparative study of theoretical predictions and simulation data identifies local structural correlations of monomers as the origin for the onset of glassy slow dynamics. It is also shown that the chain connectivity causes the polymer-specific long-time anomalies of the α process, which manifest themselves in the subdiffusive monomer mean-square displacement. Thus, the widely used picture of polymer transport in unentangled melts, the Rouse model—including deviations due to finite N—emerges from our first-principles approach (see Appendix B).

On the other hand, we also found deviations between theoretical and simulation results. Though probably not directly related to the glass transition (see the end of Sec. V D), the most noticeable disagreement occurs in the collective density fluctuations on the length scale of a chain, $q \approx q_C$ (Fig. 3). This disagreement might explain why our theory underestimates T_c ($T_c^{MCT} \approx 0.277 < T_c^{MD} \approx 0.45$). There are discernible

slow modes at $q \approx q_C$, not accounted for by our theory, which appear to couple to the relaxation at other wave vectors. The only way in which our theory can compensate this additional coupling is by making the cage effect stronger, i.e., by increasing the first peak of $S(q)$ via a decrease of T_c^{MCT}. Another possible source for the underestimation of T_c^{MCT} could result from the neglect of the triple direct correlation functions c_3 in our theoretical calculations. It was found from a MCT analysis for a model of *ortho*-terphenyl that including c_3 considerably increases T_c^{MCT} [36]. For our polymer model, c_3 has been determined from simulations in Ref. [16], and in principle it would be rather straightforward to take them into account in our theory. Unfortunately, the statistical accuracy of the simulated c_3 was not sufficient to allow for a meaningful test to investigate to what extent the inclusion of c_3 affects the value of T_c^{MCT}.

Inspection of Fig. 10 implies that the disagreement found in the theoretical predictions—the one in the collective dynamics at $q \approx q_C$ and the other in $g_C(t)$ concerning the anomalous c.m. dynamics—might be somehow related, since these are the features for which our theory does not work well. Superficially, this conjecture agrees with the physics discussed in Ref. [35]. There, the anomalous c.m. MSD is connected to the polymer coils interacting as spheres of radius of gyration R_g, and the dynamics at $q_C \approx 2\pi/R_g$ reflects the polymer packing. This implies that taking into account the spatial correlation of c.m.'s through the c.m. structure factor $S_C(q)$ might improve the theoretical results for $\phi(q,t)$ at $q \approx q_C$ and $g_C(t)$. Implementing this idea is rather straightforward (see Ref. [37] for a related problem). However, no improvement was obtained in our case, certainly because $S_C(q)$ at q_C is already close to 1 (see the inset of Fig. 1). Thus, the static coupling between the c.m.'s in our model is very weak. Furthermore, their dynamic coupling is also found to be weak, as evidenced by the close agreement of their coherent and incoherent intermediate scattering functions at q_C [38]. At present, it is not clear how to improve the theory to account for the deviations observed in the collective dynamics at $q \approx q_C$ and in the c.m. MSD $g_C(t)$. It would be interesting to investigate to what extent such features are universal or model dependent. Only comparison with other models can elucidate this point.

There is another interesting related issue concerning the collective dynamics at $q \approx q_C$. One observes from comparing Fig. 3(b) with the lower inset of Fig. 10 that the simulation result for the ratio τ_{q_C}/τ_{q^*} of the α relaxation time at q_C to the one at the structure factor peak position q^* decreases with decreasing T toward T_c^{MD}. A similar feature was observed in a simulation result for a model of *ortho*-terphenyl which also exhibits some unusual properties at intermediate wave numbers corresponding to q_C of the present polymer model [37]. A similar T dependence of the ratio τ_q/τ_{q^*} at intermediate q range ($\approx 0.4q^*$) was also found in the coherent neutron-scattering results for a real polymer system [39]. As discussed in some detail in Ref. [37], such T dependence of the ratio of the α relaxation times is beyond the implication of MCT. Thus, further investigations are necessary for a comprehensive understanding of the as yet theoretically unexplained dynamics at intermediate wave numbers which are observable in simulation and experimental data for polymer systems.

ACKNOWLEDGMENTS

Financial support by the DFG and MENRT (IRTG "Soft Matter"), the IUF, the DAAD (Grant No. D/00/07994), the ESF SUPERNET Program, and a Grant-in-Aid for scientific research from the Ministry of Education, Culture, Sports, Science and Technology of Japan (Grant No. 17740282) is gratefully acknowledged.

APPENDIX A: DERIVATION OF THE MCT EQUATIONS OF MOTION

This appendix is devoted to the derivation of the MCT equations of motion for general flexible (in the sense that constituent atoms are bonded by some nonrigid potential) molecules. Additional approximations, introduced specifically for handling polymeric systems, are discussed in the main text.

1. Zwanzig-Mori equation of motion

We start from the derivation of an exact equation of motion for the site-site density correlators $F_{ab}(q,t) = \langle \rho_a(\mathbf{q})^* e^{i\mathcal{L}t} \rho_b(\mathbf{q}) \rangle / n$ based on the Zwanzig-Mori projection-operator formalism [21]. Here, $\mathcal{L}$ denotes the Liouville operator

$$i\mathcal{L} = \sum_{i=1}^{n} \sum_{a=1}^{N} \mathbf{v}_i^a \cdot \frac{\partial}{\partial \mathbf{r}_i^a} - \frac{1}{m} \sum_{i,j=1}^{n} \sum_{a,b=1}^{N} \frac{\partial U(|\mathbf{r}_i^a - \mathbf{r}_j^b|)}{\partial \mathbf{r}_i^a} \cdot \frac{\partial}{\partial \mathbf{v}_i^a}, \tag{A1}$$

where $\mathbf{r}_i^a$ ($\mathbf{v}_i^a$) denotes the position (velocity) of the site a in the ith molecule. The interaction potential $U(r)$ comprises both the intra- and intermolecular contributions (see Sec. II).

To derive the exact equation for $F_{ab}(q,t)$, let us also introduce the longitudinal current density fluctuations $j_a(\mathbf{q}) = \sum_{i=1}^{n} v_{i,z}^a e^{i\mathbf{q}\cdot\mathbf{r}_i^a}$ where the wave vector $\mathbf{q}$ is chosen along the z axis, and $v_{i,z}^a(t)$ denotes the z component of the velocity. $\rho_a(\mathbf{q})$ and $j_a(\mathbf{q})$ satisfy the continuity equation

$$\dot{\rho}_a(\mathbf{q}) = i\mathcal{L}\rho_a(\mathbf{q}) = iqj_a(\mathbf{q}), \tag{A2}$$

in which the overdot denotes the time derivative. For flexible-molecule systems whose kinetic energy reads $\sum_{i,a} m(\mathbf{v}_i^a)^2/2$, the static longitudinal current correlation function is given by

$$J_{ab}(q) = \frac{1}{n} \langle j_a(\mathbf{q})^* j_b(\mathbf{q}) \rangle = \delta_{ab} v^2, \tag{A3}$$

due to the equipartition theorem. Unlike the case for rigid molecules [40], there is no off-diagonal element and no wave-number dependence in $J_{ab}(q)$.

Let us introduce two row vectors $\boldsymbol{\rho}(\mathbf{q})$ and $\mathbf{j}(\mathbf{q})$, whose components are $\rho_a(\mathbf{q})$ and $j_a(\mathbf{q})$, respectively. Combining $\boldsymbol{\rho}(\mathbf{q})$ and $\mathbf{j}(\mathbf{q})$ to form a new row vector $\mathbf{C}(\mathbf{q}) \equiv (\boldsymbol{\rho}(\mathbf{q})\mathbf{j}(\mathbf{q}))$,

we introduce the following projection operator $\mathcal{P}$ which acts on some row vector $\mathbf{X}(\mathbf{q})$:

$$\mathcal{P}\mathbf{X} \equiv \mathbf{C}(\mathbf{C},\mathbf{C})^{-1}(\mathbf{C},\mathbf{X}). \tag{A4}$$

Here, the inner product of two row vectors $\mathbf{A}_1$ and $\mathbf{A}_2$ will be defined as the canonical ensemble average $(\mathbf{A}_1,\mathbf{A}_2) \equiv \langle \mathbf{A}_1^\dagger \mathbf{A}_2\rangle/n$, in which $\mathbf{A}_1^\dagger$ denotes a column vector adjoint to $\mathbf{A}_1$, and the factor $1/n$ is a matter of convention. The matrix $(\mathbf{C},\mathbf{C})$ can thus be expressed in terms of the site-site static correlation functions as

$$(\mathbf{C},\mathbf{C}) = \begin{pmatrix} \mathbf{S}(q) & 0 \\ 0 & \mathbf{J}(q) \end{pmatrix}, \tag{A5}$$

and its inverse is trivially given in terms of $\mathbf{S}^{-1}(q)$ and $\mathbf{J}^{-1}(q)$.

With the projection operator $\mathcal{P}$ so defined, the standard procedure of the Zwanzig-Mori formalism leads to the following equation of motion for $F_{ab}(q,t)$:

$$\ddot{F}_{ab}(q,t) + \sum_{x=1}^{N} \Omega_{ax}^2(q) F_{xb}(q,t) + \sum_{x=1}^{N} \int_0^t dt' M_{ax}(q,t-t') \dot{F}_{xb}(q,t') = 0. \tag{A6}$$

Here the characteristic frequency matrix reads

$$\Omega_{ab}^2(q) = q^2 v^2 S_{ab}^{-1}(q), \tag{A7}$$

and the formal expression for the site-site memory kernel $M_{ab}(q,t)$ is given by

$$M_{ab}(q,t) = \frac{1}{nv^2}\langle f_a(\mathbf{q})^* \exp(i\mathcal{Q}\mathcal{L}\mathcal{Q}t) f_b(\mathbf{q})\rangle, \tag{A8}$$

in terms of the fluctuating random force

$$f_a(\mathbf{q}) = \dot{j}_a(\mathbf{q}) - iqv^2 \sum_\nu \rho_\nu(\mathbf{q}) S_{\nu a}^{-1}(q), \tag{A9}$$

which evolves with the generator $\mathcal{Q}\mathcal{L}\mathcal{Q}$, where $\mathcal{Q} \equiv 1 - \mathcal{P}$. So far, no approximation has been invoked, and the above equation for $F_{ab}(q,t)$ is formally exact.

2. Mode-coupling approximation

The basic idea behind the mode-coupling theory is that the fluctuation of a given dynamical variable decays, at intermediate and long times, predominantly into pairs of hydrodynamic modes associated with quasiconserved dynamical variables. It is reasonable to expect that the decay of the memory function at intermediate and long times is dominated by those mode correlations which have the longest relaxation times. The sluggishness of the structural relaxation processes in glass-forming systems suggests that the slow decay of the memory function at long times is basically due to couplings to wave-vector-dependent pair density modes of the form $A_{\lambda\mu}(\mathbf{k},\mathbf{p}) \equiv \rho_\lambda(\mathbf{k})\rho_\mu(\mathbf{p})$. The simplest way to extract such a slowly decaying part is to introduce another projection operator $\mathcal{P}_2$ which projects any variable onto the subspace spanned by $A_{\lambda\mu}(\mathbf{k},\mathbf{p})$. Translational invariance of the system implies that the only $A_{\lambda\mu}(\mathbf{k},\mathbf{p})$ whose inner products with a dynamical variable $X(\mathbf{q})$ are nonzero are for the wave vectors $\mathbf{p}$ satisfying $\mathbf{p}=\mathbf{q}-\mathbf{k}$. From here on, we denote by $A_{\lambda\mu}$ those $A_{\lambda\mu}(\mathbf{k},\mathbf{p})$ in which $\mathbf{p}=\mathbf{q}-\mathbf{k}$, and we define

$$\mathcal{P}_2 X \equiv \frac{1}{2}\sum_{\mathbf{k}} \sum_{\lambda,\mu,\lambda',\mu'} A_{\lambda\mu}(A_{\lambda\mu},A_{\lambda'\mu'})^{-1}(A_{\lambda'\mu'},X). \tag{A10}$$

Here the factor 1/2 is to avoid the double counting in the summation over the wave vectors, and the inverse is defined via

$$\sum_{\lambda',\mu'} (A_{\lambda\mu},A_{\lambda'\mu'})(A_{\lambda'\mu'},A_{\lambda''\mu''})^{-1} = \delta_{\lambda\lambda''}\delta_{\mu\mu''}. \tag{A11}$$

It is readily verified that $\mathcal{P}_2$ is idempotent and Hermitian.

The first approximation in the mode-coupling approach thus corresponds to replacing the time-evolution operator $\exp(i\mathcal{Q}\mathcal{L}\mathcal{Q}t)$ by its projection on the subspace spanned by $A_{\lambda\mu}$: $\exp(i\mathcal{Q}\mathcal{L}\mathcal{Q}t) \approx \mathcal{P}_2 \exp(i\mathcal{Q}\mathcal{L}\mathcal{Q}t)\mathcal{P}_2$. Under this approximation, the memory function reads

$$M_{ab}(q,t) = \frac{1}{nv^2}\langle \mathcal{P}_2 f_a(\mathbf{q})^* \exp(i\mathcal{Q}\mathcal{L}\mathcal{Q}t)\mathcal{P}_2 f_b(\mathbf{q})\rangle. \tag{A12}$$

The second approximation is to factorize averages of products, evolving in time with the generator $\mathcal{Q}\mathcal{L}\mathcal{Q}$, into products of averages formed with variables evolving with $\mathcal{L}$ (factorization approximation):

$$\frac{1}{n^2}\langle \rho_\lambda(\mathbf{k})^* \rho_\mu(\mathbf{p})^* e^{i\mathcal{Q}\mathcal{L}\mathcal{Q}t} \rho_{\lambda'}(\mathbf{k})\rho_{\mu'}(\mathbf{p})\rangle \approx F_{\lambda\lambda'}(k,t)F_{\mu\mu'}(p,t). \tag{A13}$$

Specializing this approximation to $t=0$, it follows from Eq. (A11) that the denominator in Eq. (A10) is given by

$$(A_{\lambda\mu},A_{\lambda'\mu'})^{-1} = \frac{1}{n} S_{\lambda\lambda'}^{-1}(k) S_{\mu\mu'}^{-1}(p). \tag{A14}$$

Let us obtain the explicit expression for the projected random force,

$$\mathcal{P}_2 f_a(\mathbf{q}) = \mathcal{P}_2 \dot{j}_a(\mathbf{q}) - iqv^2 \sum_\nu [\mathcal{P}_2 \rho_\nu(\mathbf{q})] S_{\nu a}^{-1}(q). \tag{A15}$$

To this end, we need to evaluate triple correlations $(A_{\lambda\mu},\dot{j}_a(\mathbf{q}))$ and $(A_{\lambda\mu},\rho_\nu(\mathbf{q}))$. The former can be expressed as

$$(\rho_\lambda(\mathbf{k})\rho_\mu(\mathbf{p}),\dot{j}_a(\mathbf{q})) = ik_z \frac{1}{n}\langle j_\lambda^*(\mathbf{k})\rho_\mu^*(\mathbf{p}) j_a(\mathbf{q})\rangle + ip_z \frac{1}{n}\langle \rho_\lambda^*(\mathbf{k}) j_\mu^*(\mathbf{p}) j_a(\mathbf{q})\rangle, \tag{A16}$$

where we have used the relation $\langle A\dot{B}\rangle = -\langle \dot{A}B\rangle$ and the continuity equation (A2). k_z (p_z) denotes the z component of the vector $\mathbf{k}$ ($\mathbf{p}$). Since $\langle v_{i,z}^a v_{j,z}^b\rangle = \delta_{ij}\delta_{ab}v^2$, it holds that

$\langle j_\lambda^*(\mathbf{k})\rho_\mu^*(\mathbf{p})j_a(\mathbf{q})\rangle/n=\delta_{a\lambda}v^2S_{\lambda\mu}(p)$ and $\langle\rho_\lambda^*(\mathbf{k})j_\mu^*(\mathbf{p})j_a(\mathbf{q})\rangle/n=\delta_{a\mu}v^2S_{\lambda\mu}(k)$, leading to

$$(\rho_\lambda(\mathbf{k})\rho_\mu(\mathbf{p}),\dot{j}_a(\mathbf{q}))=ik_z\delta_{a\lambda}v^2S_{\lambda\mu}(p)+ip_z\delta_{a\mu}v^2S_{\lambda\mu}(k). \tag{A17}$$

The other triple correlation can be expressed in terms of the three-site static structure factor:

$$(\rho_\lambda(\mathbf{k})\rho_\mu(\mathbf{p}),\rho_\nu(\mathbf{q}))=\frac{1}{n}\langle\rho_\lambda(\mathbf{k})^*\rho_\mu(\mathbf{p})^*\rho_\nu(\mathbf{q})\rangle\equiv S_{\lambda\mu\nu}(\mathbf{k},\mathbf{p},\mathbf{q}). \tag{A18}$$

In the present study, the convolution approximation developed in Ref. [40] will be employed:

$$S_{\lambda\mu\nu}(\mathbf{k},\mathbf{p},\mathbf{q})\approx\sum_\sigma S_{\lambda\sigma}(k)S_{\mu\sigma}(p)S_{\nu\sigma}(q). \tag{A19}$$

Using these results, we finally obtain

$$\mathcal{P}_2f_a(\mathbf{q})=-\frac{iv^2}{n}\sum_{\mathbf{k}}\sum_\lambda k_z[\delta_{\lambda a}-S_{\lambda a}^{-1}(k)]\rho_\lambda(\mathbf{k})\rho_a(\mathbf{p})$$
$$=-\frac{i\rho v^2}{n}\sum_{\mathbf{k}}\sum_\lambda k_z[c_{\lambda a}^{\mathrm{intra}}(k)+c_{\lambda a}(k)]\rho_\lambda(\mathbf{k})\rho_a(\mathbf{p}). \tag{A20}$$

Here, $c_{ab}^{\mathrm{intra}}(q)=[\delta_{ab}-w_{ab}^{-1}(q)]/\rho$ denotes the *intramolecular* direct correlation function [41], whereas $c_{ab}(q)$ is the *intermolecular* one defined in Eq. (14). Thus, the projected random force naturally comprises the intramolecular as well as intermolecular contributions.

The MCT expression for $M_{ab}(q,t)$ can be obtained by substituting Eq. (A20) into Eq. (A12) and then invoking the factorization approximation (A13), but let us make here a comment on the intramolecular contribution. Within the same approach outlined above, one can derive the MCT expression for the memory kernel for the site-site *transverse* current density correlator, whose $q\to0$ limit is related to the shear-stress autocorrelation function $G(t)$ [21]. It is well known for unentangled polymer chains that $G(t)$ exhibits a power-law decay $\sim t^{-1/2}$ for long times. According to the Rouse theory, this polymer-specific decay in $G(t)$ is accounted for by the intrachain (or Rouse-mode) contributions [2]. However, we found that our intramolecular contributions given in terms of c^{intra} do not lead to this Rouse model result for $G(t)$. This implies that a completely different kind of approach is necessary for a proper treatment of the intramolecular contributions in the coherent moduli. Indeed, we found a reasonable approach starting from a different projection operator for the intramolecular forces, which reproduces the Rouse model result for $G(t)$. This issue, however, will not be investigated further here, and will be studied in a forthcoming presentation. Let us only mention that (i) even with the inclusion of such intramolecular contributions to the random force or to the memory kernel, we confirmed that all the theoretical results presented in the main text are not much affected, and (ii) neglecting intramolecular contributions to the fluctuating force does not mean that intramolecular couplings are completely discarded in our theory, since the intrachain static correlations are properly taken into account via $w_{ab}(q)$.

The following expression for $\mathcal{P}_2f_a(\mathbf{q})$ will therefore be employed in the present work:

$$\mathcal{P}_2f_a(\mathbf{q})=-\frac{i\rho v^2}{n}\sum_{\mathbf{k}}\sum_\lambda(\hat{\mathbf{q}}\cdot\mathbf{k})c_{\lambda a}(k)\rho_\lambda(\mathbf{k})\rho_a(\mathbf{p}), \tag{A21}$$

in which we have expressed k_z as $\hat{\mathbf{q}}\cdot\mathbf{k}$ with $\hat{\mathbf{q}}=\mathbf{q}/q$. With the use of the factorization approximation (A13), this leads to

$$M_{ab}(q,t)=\frac{\rho v^2}{(2\pi)^3}\sum_{\lambda,\mu=1}^N\int d\mathbf{k}[(\hat{\mathbf{q}}\cdot\mathbf{k})^2c_{\lambda a}(k)c_{\mu b}(k)F_{\lambda\mu}(k,t)$$
$$\times F_{ab}(p,t)+(\hat{\mathbf{q}}\cdot\mathbf{k})$$
$$\times(\hat{\mathbf{q}}\cdot\mathbf{p})c_{\lambda a}(k)c_{\mu b}(p)F_{\lambda b}(k,t)F_{a\mu}(p,t)]. \tag{A22}$$

3. MCT equations for a tagged molecule's correlator

The MCT equations of motion for a tagged molecule (labeled s) can be derived in a similar manner, and only the outline of the derivation and resulting equations will be presented in the following. The Zwanzig-Mori equation for the tagged molecule's density correlator $F_{ab}^{\mathrm{s}}(q,t)=\langle\rho_a^{\mathrm{s}}(\mathbf{q})e^{i\mathcal{L}t}\rho_b^{\mathrm{s}}(\mathbf{q})\rangle$ is obtained from the projection operator $\mathcal{P}^{\mathrm{s}}$ onto $\rho_a^{\mathrm{s}}(\mathbf{q})$ and $j_a^{\mathrm{s}}(\mathbf{q})=v_{\mathrm{s},z}^a e^{i\mathbf{q}\cdot\mathbf{r}_{\mathrm{s}}^a}$, and is given by

$$\ddot{F}_{ab}^{\mathrm{s}}(q,t)+\sum_{x=1}^N\Omega_{ax}^{\mathrm{s}2}(q)F_{xb}^{\mathrm{s}}(q,t)$$
$$+\sum_{x=1}^N\int_0^t dt'M_{ax}^{\mathrm{s}}(q,t-t')\dot{F}_{xb}^{\mathrm{s}}(q,t')=0. \tag{A23}$$

Here the characteristic frequency matrix reads

$$\Omega_{ab}^{\mathrm{s}2}(q)=q^2v^2w_{ab}^{-1}(q), \tag{A24}$$

and the formal expression for the memory kernel is given by

$$M_{ab}^{\mathrm{s}}(q,t)=\frac{1}{v^2}\langle f_a^{\mathrm{s}}(\mathbf{q})^*\exp(i\mathcal{Q}^{\mathrm{s}}\mathcal{L}\mathcal{Q}^{\mathrm{s}}t)f_b^{\mathrm{s}}(\mathbf{q})\rangle, \tag{A25}$$

in terms of the fluctuating random force evolving with $\mathcal{Q}^{\mathrm{s}}\mathcal{L}\mathcal{Q}^{\mathrm{s}}$ ($\mathcal{Q}^{\mathrm{s}}\equiv1-\mathcal{P}^{\mathrm{s}}$)

$$f_a^{\mathrm{s}}(\mathbf{q})=\dot{j}_a^{\mathrm{s}}(\mathbf{q})-iqv^2\sum_\nu\rho_\nu^{\mathrm{s}}(\mathbf{q})w_{\nu a}^{-1}(q). \tag{A26}$$

The memory kernel under the mode-coupling approximation reads

$$M_{ab}^{\mathrm{s}}(q,t)=\frac{1}{v^2}\langle\mathcal{P}_2^{\mathrm{s}}f_a^{\mathrm{s}}(\mathbf{q})^*\exp(i\mathcal{Q}^{\mathrm{s}}\mathcal{L}\mathcal{Q}^{\mathrm{s}}t)\mathcal{P}_2^{\mathrm{s}}f_b^{\mathrm{s}}(\mathbf{q})\rangle. \tag{A27}$$

Here the operator $\mathcal{P}_2^{\mathrm{s}}$ projects any variable onto the subspace spanned by the pair density modes $A_{\lambda\mu}^{\mathrm{s}}(\mathbf{k},\mathbf{p})=\rho_\lambda^{\mathrm{s}}(\mathbf{k})\rho_\mu(\mathbf{p})$ formed by the tagged molecule's density fluctuations and

collective ones. Adopting the convolution approximation relevant here [40],

$$\langle \rho_\lambda^s(\mathbf{k})^* \rho_\mu(\mathbf{p})^* \rho_\nu^s(\mathbf{q})\rangle \approx \sum_\sigma w_{\lambda\sigma}(k)\rho h_{\mu\sigma}(p) w_{\nu\sigma}(q), \tag{A28}$$

one obtains for the projected random force

$$\begin{aligned}\mathcal{P}_2^s f_s^a(\mathbf{q}) &= -i\frac{\rho v^2}{n}\sum_{\mathbf{k}}\sum_{\lambda,\mu,\nu}\{k_z[\delta_{\lambda a} - w_{\lambda a}^{-1}(k)] \\ &\quad + p_z\delta_{\lambda a}\} w_{a\nu}(p) c_{\nu\mu}(p)\rho_\lambda^s(\mathbf{k})\rho_\mu(\mathbf{p}) \\ &= -i\frac{\rho v^2}{n}\sum_{\mathbf{k}}\sum_{\lambda,\mu,\nu}[k_z\rho c_{\lambda a}^{\text{intra}}(k) + p_z\delta_{\lambda a}] \\ &\quad \times [\mathbf{I} - \rho \mathbf{c}^{\text{intra}}(p)]^{-1}_{a\nu} c_{\nu\mu}(p)\rho_\lambda^s(\mathbf{k})\rho_\mu(\mathbf{p}),\end{aligned} \tag{A29}$$

where in the final equality the intramolecular structure factor is expressed in terms of c^{intra}. Again, intramolecular contributions given in terms of c^{intra} will be neglected here, which leads to

$$\mathcal{P}_2^s f_a^s(\mathbf{q}) = -\frac{i\rho v^2}{n}\sum_{\mathbf{k}}\sum_{\lambda}(\hat{\mathbf{q}}\cdot\mathbf{p})c_{a\lambda}(p)\rho_a^s(\mathbf{k})\rho_\lambda(\mathbf{p}). \tag{A30}$$

All the theoretical results presented in the main text are not much affected by this neglect, since $w_{ab}(q)$ for microscopic wave vectors, in particular, near the peak position q^* of the static structure factor $S(q)$, are close to diagonal [16], in which case $c_{ab}^{\text{intra}}(q)\approx 0$ holds. In addition, our derivation of the Rouse model presented in Appendix B is not altered since the relevant memory kernel there, $\hat{m}_{\lambda=0}(t)$, is formed by the summation $\Sigma_{a=1}^N \mathcal{P}_2^s f_a^s(\vec{q}\to 0)$ of the projected random forces in the small-wave-vector limit, for which both Eqs. (A29) and (A30) yield the identical expression. Under the factorization approximation

$$\frac{1}{n}\langle \rho_a^s(\mathbf{k})^* \rho_\lambda(\mathbf{p})^* e^{i\mathcal{Q}^s\mathcal{L}\mathcal{Q}^s t}\rho_b^s(\mathbf{k})\rho_\mu(\mathbf{p})\rangle \approx F_{ab}^s(k,t)F_{\lambda\mu}(p,t), \tag{A31}$$

substituting Eq. (A30) into Eq. (A27) finally yields

$$\begin{aligned}M_{ab}^s(q,t) &= \frac{\rho v^2}{(2\pi)^3}\sum_{\lambda,\mu=1}^N \int d\mathbf{k}(\hat{\mathbf{q}}\cdot\mathbf{p})^2 c_{a\lambda}(p)c_{b\mu}(p) \\ &\quad \times F_{ab}^s(k,t)F_{\lambda\mu}(p,t).\end{aligned} \tag{A32}$$

APPENDIX B: DERIVATION OF THE ROUSE MODEL

In this appendix, we show that our microscopic formulation for the polymer dynamics based on MCT reduces to the Rouse model in the asymptotic limit of large degrees of polymerization N. Implications of our theory in this limit for the Rouse-mode correlators in the β and α relaxation regimes and possible finite-N corrections are also discussed.

1. MCT equations for mean-square displacements

We start by deriving the MCT equations for monomer MSDs,

$$\Delta r_{ab}^2(t) \equiv \delta r_{ab}^2(t) - \delta r_{ab}^2(0) \quad \text{with} \quad \delta r_{ab}^2(t) = \langle [\mathbf{r}_a(t) - \mathbf{r}_b(0)]^2\rangle. \tag{B1}$$

Notice that the c.m. MSD $g_C(t)$ and the monomer-averaged one $g_M(t)$ introduced in Sec. IV C can be expressed in terms of $\Delta r_{ab}^2(t)$ as

$$g_C(t) = \frac{1}{N^2}\sum_{a,b=1}^N \Delta r_{ab}^2(t), \tag{B2}$$

$$g_M(t) = \frac{1}{N}\sum_{a=1}^N \Delta r_{aa}^2(t) = \frac{1}{N}\text{Tr}[\Delta r^2(t)]. \tag{B3}$$

Since $F_{ab}^s(q\to 0,t) = 1 - q^2\delta r_{ab}^2(t)/6 + O(q^4)$ [see Eq. (36)], the Zwanzig-Mori equation for $\Delta r_{ab}^2(t)$ can be derived from the small-q behavior of Eq. (37),

$$\begin{aligned}&\frac{1}{v^2}\partial_t^2\Delta r_{ab}^2(t) + q^2\sum_{x=1}^N w_{ax}^{-1}(q\to 0)\Delta r_{xb}^2(t) \\ &\quad + \sum_{x=1}^N \int_0^t dt' m_{ax}(t-t')\partial_{t'}\Delta r_{xb}^2(t') = 6\delta_{ab},\end{aligned} \tag{B4}$$

with the memory kernel $m_{ab}(t) = \lim_{q\to 0} q^2\Sigma_x w_{ax}^{-1}(q)m_{xb}(t)$ [see Eqs. (39) and (40)]:

$$m_{ab}(t) = \frac{\rho_m}{6\pi^2}\int dk\, k^4 S(k)c(k)^2 F_{ab}^s(k,t)\phi(k,t). \tag{B5}$$

In Eq. (B4), the term $q^2 w_{ab}^{-1}(q\to 0)$ has to be kept since $w_{ab}(q=0)=1$ is singular and its inverse does not exist. For $g_C(t)$, a somewhat simplified equation can be derived by taking $(1/N^2)\Sigma_{a,b}$ of Eq. (B4) and noticing that $\lim_{q\to 0} q^2\Sigma_a w_{ax}^{-1}(q) = 0$:

$$\frac{1}{v^2}\partial_t^2 g_C(t) + \frac{1}{N^2}\sum_{a,x,b=1}^N \int_0^t dt' m_{ax}(t-t')\partial_{t'}\Delta r_{xb}^2(t') = \frac{6}{N}. \tag{B6}$$

2. Derivation of the Rouse model as asymptotic solution

In general, no simplification of the complicated couplings in the motions of all monomers is possible, as an exact diagonalization of the integro-differential equations for the matrix $\Delta r_{ab}^2(t)$ is required. Only for long times and large degrees of polymerization N is an asymptotic solution possible, and it is presented in the following. It rests upon the property of the memory functions $m_{ab}(t)$ in Eq. (B5) that they are cut off by the collective density fluctuations. The slowest collective correlator $\phi(q,t)$ is connected with the average monomer

separation and lies at the position q^* of the peak of $S(q)$ (see Sec. V A). Thus, at long times, the tagged polymer's density correlator $F^s_{ab}(q,t)$ at the (asymptotically N-independent) wave vector q^* dominates the memory functions. It is bounded by the intrachain structure factor at that wave vector, i.e., $w_{ab}(q^*) > F^s_{ab}(q^*,t)$ [in the sense that $w_{ab}(q^*) - F^s_{ab}(q^*,t)$ is positive definite]. As long as $w_{ab}(q^*)$ on this length scale contains no anomalous correlations extending over large monomer separations, i.e., $w_{ab}(q^*) \to 0$ for $|a-b| \to \infty$, the same property holds for the memory function as well: $m_{ab}(t) \to 0$ for $|a-b| \to \infty$. This property, and that $m_{ab}(t)$ decays to zero for times longer than τ_{q^*}, the structural relaxation time, are the central ingredients to the derivation of the Rouse model within our approach. Note that the above reasoning also holds if the role of the microscopic wave vector q^* is replaced by some other wave vector $q^\dagger$, as long as $q^\dagger$ is characteristic of local motion and asymptotically N independent. Thus, the following reasoning also applies to high temperature, where, as discussed in Sec. V D, the slowest collective mode in the simulation result is found to lie at $q \approx q_C$ [42].

For long times, $t \to \infty$, Eq. (B6) is solved by a uniform increase of all MSDs following the c.m. motion:

$$g_C(t) \to 6Dt \quad \text{and} \quad \delta r^2_{ab}(t) \to g_C(t) + O(t^x), \tag{B7}$$

where the Markovian limit in the memory function requires $t \gg \tau_{q^*}$. Below, we will determine the leading correction that exhibits a power-law behavior with the exponent $x = 1/2$. As explained above, the site dependence of $m_{ab}(t)$ for long times is dominated by the tagged polymer's density fluctuations at microscopic wave vectors. Therefore, the summation over site indices and consecutive k integration will asymptotically become N independent, and the diffusion constant D scales as

$$D = \frac{k_B T}{N\zeta} \quad (N \to \infty), \tag{B8}$$

with the (asymptotically N-independent) friction coefficient ζ determined by

$$\zeta/k_B T = \frac{\rho_m}{6\pi^2} \int_0^\infty dt \int dk\, k^4 S(k) c^2(k) \left(\frac{1}{N} \sum_{a,b=1}^{N} F^s_{ab}(k,t) \right) \phi(k,t). \tag{B9}$$

We confirmed that the Gaussian chains studied in Ref. [15] follows the asymptotic law (B8) for large N.

In considering internal-mode contributions to the monomer MSD in the limit of $N \to \infty$, chain-end effects can be neglected, and the structure of the various matrices in Eq. (B4) simplifies. We can assume that they depend only on the difference of indices, $s = a-b$ (characteristic of Toeplitz matrices [43]), and we define, e.g., $\Delta r^2_{(s=a-b)}(t) = \Delta r^2_{ab}(t)$. This assumption neglects monomer correlations caused by chain ends and does not hold, e.g., for isolated self-avoiding-walk polymers in good solvents, whose end regions are slightly less swollen than middle portions. Similar correlations have recently been discovered also in long-chain polymer melts, but the amplitude is much weaker than in dilute solution [44]. Here, as a first step, we assume that such nontrivial correlations are absent.

For the monomer-averaged MSD, it suffices to obtain the distribution of the internal modes since $g_M(t)$ in Eq. (B3) is expressed as the trace of the matrix $\Delta r^2_{ab}(t)$, where only the eigenvalues of the internal modes enter. The distribution in the $N \to \infty$ limit can be found by assuming periodic boundary conditions and performing a Fourier transform. Transformed quantities like

$$\widehat{\Delta r^2_\lambda}(t) = \sum_{s=-\infty}^{\infty} e^{i\lambda s} \Delta r^2_{(s)}(t) \tag{B10}$$

will be marked by a caret. Notice that $g_C(t) = (1/N)\widehat{\Delta r^2_{\lambda=0}}(t)$ and $g_M(t) = (1/N)\Sigma_\lambda \widehat{\Delta r^2_\lambda}(t)$ hold, so that the internal-mode contribution to the monomer-averaged MSD is given by $g_M(t) - g_C(t) = (1/N)\Sigma_{\lambda \neq 0} \widehat{\Delta r^2_\lambda}(t)$. In the asymptotic $N \to \infty$ limit, the monomer-averaged MSD follows from the density of states of internal modes via [43]

$$g_M(t) - g_C(t) \to \int_{-\pi}^{\pi} \frac{d\lambda}{2\pi} \widehat{\Delta r^2_\lambda}(t). \tag{B11}$$

Here and in the following, $\lambda \neq 0$ will be assumed unless stated otherwise.

The equation of motion for $\widehat{\Delta r^2_\lambda}(t)$ is obtained from Eq. (B4) via Fourier transformation, recognizing that matrix products, owing to the assumption of the dependence on the index difference only, become convolution and turn into simple products after Fourier transformation:

$$\frac{1}{v^2} \partial_t^2 \widehat{\Delta r^2_\lambda}(t) + \hat{\Gamma}_\lambda \widehat{\Delta r^2_\lambda}(t) + \int_0^t dt' \hat{m}_\lambda(t-t') \partial_{t'} \widehat{\Delta r^2_\lambda}(t') = 6. \tag{B12}$$

Here we have introduced

$$\hat{\Gamma}^{-1}_\lambda \equiv \lim_{q \to 0} \frac{\hat{w}_\lambda(q)}{q^2} = -\frac{1}{6} \sum_{s=-\infty}^{\infty} e^{i\lambda s} \delta r^2_{(s)}(0), \tag{B13}$$

and the transformed memory kernel is given by

$$\hat{m}_\lambda(t) = \frac{\rho_m}{6\pi^2} \int dk\, k^4 S(k) c^2(k) \hat{F}^s_\lambda(k,t) \phi(k,t). \tag{B14}$$

Equations (B11) and (B12) yield the N-independent growth of the monomer-averaged MSD resulting from the internal modes, whose spectrum will be determined to lowest order in the mode parameter λ. The Gaussian approximation will be assumed for the large-separation behavior in $\delta r^2_{(s=a-b)}(0)$ [44], so that the small-λ properties of $\hat{\Gamma}_\lambda$ can be found from

$$\hat{\Gamma}^{-1}_\lambda \approx -\frac{1}{6} \sum_{s=-\infty}^{\infty} e^{i\lambda s} |s| \sigma_s^2 \to \frac{\sigma_s^2}{3\lambda^2}. \tag{B15}$$

Here σ_s denotes the statistical segment length. At the same time, the memory kernel is Taylor expanded for small λ, and then a Markovian approximation (see the next section) is performed,

$$\hat{m}_\lambda(t) \approx \left(\int_0^\infty dt\, \hat{m}_{\lambda=0}(t) \right) \delta(t) = (\zeta/k_B T)\delta(t), \quad \text{(B16)}$$

to derive the long-time behavior. It is justified, as discussed above, because the memory kernel is dominated by microscopic wave vectors, where the summation over $s=a-b$ converges rapidly and an expansion in λ is possible. In Eq. (B16) only the lowest order in λ is retained, which is given by the friction coefficient from Eq. (B9) of the c.m. motion. Neglecting the inertia term for long times, we find from Eq. (B12) for the small-λ modes

$$\frac{\zeta}{k_B T}\partial_t \widehat{\Delta r}^2_\lambda(t) + \frac{3\lambda^2}{\sigma_s^2}\widehat{\Delta r}^2_\lambda(t) = 6, \quad \text{(B17)}$$

with the initial value $\widehat{\Delta r}^2_\lambda(0)=0$, or equivalently

$$\frac{\zeta}{k_B T}\partial_t \widehat{\delta r}^2_\lambda(t) + \frac{3\lambda^2}{\sigma_s^2}\widehat{\delta r}^2_\lambda(t) = 0, \quad \text{(B18)}$$

whose solution reads

$$\widehat{\delta r}^2_\lambda(t) = e^{-3k_B T\lambda^2 t/\zeta\sigma_s^2}\widehat{\delta r}^2_\lambda(0), \quad \text{(B19)}$$

with $\widehat{\delta r}^2_\lambda(0) = -2\sigma_s^2/\lambda^2$. From this, the following monomer-averaged MSD follows for long times, as familiar in the Rouse model [2]:

$$g_M(t) - g_C(t) = \int_{-\pi}^{\pi} \frac{d\lambda}{2\pi}\frac{\sigma_s^2}{2\lambda^2}(1 - e^{-3k_B T\lambda^2 t/\zeta\sigma_s^2}) \rightarrow \frac{2\sigma_s^2}{\pi^{3/2}}\sqrt{\frac{3\pi^2 k_B T}{\zeta\sigma_s^2}}\sqrt{t}. \quad \text{(B20)}$$

This concludes the derivation of the Rouse model as the asymptotic large-chain-length limit of the MCT equations for a polymer chain dissolved in a melt of identical polymers. (The use of the Markovian approximation will be justified in the next section.) We find the expected scaling of the diffusion coefficient with molecular weight in Eq. (B8), the (low-lying) spectrum of eigenvalues in Eq. (B19), and the resulting anomaly in the monomer MSD, Eq. (B20). The occurring parameters can be measured from global chain properties: the friction coefficient ζ from the averaged friction kernel Eq. (B9), and the segment length σ_s from the Gaussian behavior of the equilibrium segment correlations at large separation, Eq. (B15).

3. Implications for the Rouse-mode correlators

We notice that $\widehat{\delta r}^2_\lambda(t)$ is essentially the (diagonal) Rouse-mode correlators $C_{pp}(t)$ introduced in Sec. IV C with the correspondence $\lambda \sim p/N$ since $6\Sigma_{p\geq 1}[C_{pp}(0) - C_{pp}(t)] = \Sigma_{\lambda\neq 0}[\widehat{\delta r}^2_\lambda(t) - \widehat{\delta r}^2_\lambda(0)]$ holds, from the comparison of Eqs. (49) and (B11). The difference comes from the boundary condition adopted in defining $C_{pp}(t)$ and $\widehat{\delta r}^2_\lambda(t)$. So the small-$p$ properties of the normalized Rouse-mode correlators $c_p(t) = C_{pp}(t)/C_{pp}(0)$ can be deduced from the small-λ behavior of

$$\hat{c}_\lambda(t) = \widehat{\delta r}^2_\lambda(t)/\widehat{\delta r}^2_\lambda(0). \quad \text{(B21)}$$

The equation of motion for $\hat{c}_\lambda(t)$ can be derived from Eq. (B12):

$$\frac{1}{v^2}\partial_t^2 \hat{c}_\lambda(t) + \hat{\Gamma}_\lambda \hat{c}_\lambda(t) + \int_0^t dt' \hat{m}_\lambda(t-t')\partial_{t'}\hat{c}_\lambda(t') = 0. \quad \text{(B22)}$$

The Laplace transform of this equation reads

$$-\frac{1}{v^2} z[1 + z\hat{c}_\lambda(z)] + \hat{\Gamma}_\lambda \hat{c}_\lambda(z) - \hat{m}_\lambda(z)[1 + z\hat{c}_\lambda(z)] = 0, \quad \text{(B23)}$$

where the convention $f(z) = i\int_0^\infty dt\, e^{izt} f(t)$ with $\mathrm{Im}\, z > 0$ is adopted.

Let us consider liquid states, for which there is no nonergodicity pole in the Laplace transform of correlators. (Nonergodicity parameters will be discussed below.) Then we have, from the $z\to 0$ limit of Eq. (B23), $\hat{\Gamma}_\lambda \hat{c}_\lambda(z\to 0) = \hat{m}_\lambda(z \to 0)$. Retaining only the leading-order contribution in λ for $\hat{\Gamma}_\lambda$ and $\hat{m}_\lambda$, one obtains for small λ

$$\hat{c}_\lambda(z\to 0) = \frac{\sigma_s^2}{3\lambda^2}\hat{m}_{\lambda=0}(z\to 0). \quad \text{(B24)}$$

Since $\hat{c}_\lambda(z\to 0)$ and $\hat{m}_{\lambda=0}(z\to 0)$ are proportional to their relaxation times, this implies that the relaxation time of $\hat{c}(t)$ [and hence of $\widehat{\delta r}^2_\lambda(t)$] is larger by a factor of $1/\lambda^2 \sim (N/p)^2$ than that of $\hat{m}_{\lambda=0}(t)$. This justifies the use of the Markovian approximation, which has been adopted in Eq. (B16). Since, as discussed above, the relaxation time of $\hat{m}_{\lambda=0}(t)$ is dictated by that of the coherent dynamics at microscopic wave vectors, Eq. (B24) also implies the separation of the time scale for $\hat{c}(t)$ from that for the density fluctuations at the monomer length scale.

We next turn our attention to nonergodicity parameters $\hat{f}_\lambda = \hat{c}_\lambda(t\to\infty)$ and $\hat{m}_\lambda = \hat{m}_\lambda(t\to\infty)$ in glass states. Since it holds that $\lim_{t\to\infty} f(t) = -\lim_{z\to 0} zf(z)$, one obtains from the $z\to 0$ limit of Eq. (B23) $\hat{f}_\lambda = \hat{m}_\lambda/[\hat{m}_\lambda + \hat{\Gamma}_\lambda]$. Because of Eq. (B15), we have $\hat{f}_\lambda = 1$ in leading order for small λ. This holds also at the MCT critical point, so that the critical nonergodicity parameter for $\hat{c}_\lambda(t)$ is $\hat{f}^c_\lambda = 1$. Since $\hat{c}_\lambda(t) \leq 1$, this also implies that the critical amplitude for $\hat{c}_\lambda(t)$ is zero, $\hat{h}_\lambda = 0$. Therefore, our theory predicts that, for small mode indices or in the $N\to\infty$ limit, the critical nonergodicity parameter of the Rouse-mode correlators is unity, and they do not exhibit the MCT β dynamics (see Sec. IV D).

Let us then consider the dynamics of $\hat{c}_\lambda(t)$ in the α regime, which can be described by its α master curve [see Eq. (60)]. We consider the dynamics on the α relaxation time scale t'_σ [see Eq. (57)] and write, e.g., $\hat{c}_\lambda(t) = \tilde{c}_\lambda(\tilde{t})$ with $\tilde{t} = t/t'_\sigma$ and $\hat{c}_\lambda(z) = t'_\sigma \tilde{c}_\lambda(\tilde{z})$ with $\tilde{z} = zt'_\sigma$, with a yet unspecified function $\tilde{c}_\lambda$. It then follows from Eq. (B23) that

$$-\frac{1}{v^2}\frac{\tilde{z}}{(t'_\sigma)^2}[1+\tilde{z}\tilde{c}_\lambda(\tilde{z})]+\hat{\Gamma}_\lambda\tilde{c}_\lambda(\tilde{z})-\tilde{m}_\lambda(\tilde{z})[1+\tilde{z}\tilde{c}_\lambda(\tilde{z})]=0. \tag{B25}$$

Now, the α scaling limit will be performed: $t'_\sigma\to\infty$ for $T\to T_c+$, but with $\tilde{t}$ and $\tilde{z}$ fixed [11]. We thus obtain $\hat{\Gamma}_\lambda\tilde{c}_\lambda(\tilde{z})-\tilde{m}_\lambda(\tilde{z})[1+\tilde{z}\tilde{c}_\lambda(\tilde{z})]=0$. Since $\tilde{c}_\lambda(\tilde{t}\to 0)=\hat{f}^c_\lambda$ [11] and $\hat{f}^c_\lambda=1$ for small λ as derived above, the inverse Laplace transform of this equation yields

$$\hat{\Gamma}_\lambda\tilde{c}_\lambda(\tilde{t})+\int_0^{\tilde{t}}d\tilde{t}'\,\tilde{m}_\lambda(\tilde{t}-\tilde{t}')\partial_{\tilde{t}'}\tilde{c}_\lambda(\tilde{t}')=0. \tag{B26}$$

Again, only the leading-order contribution in λ for $\hat{\Gamma}_\lambda$ and $\tilde{m}_\lambda$ will be retained. With the same reasoning as presented concerning Eq. (B24), one obtains the time-scale separation of the dynamics of $\tilde{c}_\lambda(\tilde{t})$ from that of $\tilde{m}_{\lambda=0}(\tilde{t})$. Therefore, the Markovian approximation for Eq. (B26) is justified, leading for small λ to the exponential decay of the α master curve

$$\tilde{c}_\lambda(\tilde{t})=\exp[-\tilde{t}/\tilde{\tau}_\lambda], \tag{B27}$$

with the relaxation time $\tilde{\tau}_\lambda=\tilde{\zeta}\sigma_s^2/3k_BT\lambda^2$ ($\tilde{\zeta}=\lim_{T\to T_c+}\zeta/t'_\sigma$) whose dependence on the mode index reads $1/\lambda^2\sim(N/p)^2$. Thus, our theory in the $N\to\infty$ limit yields the Rouse-model result for the α master curves for the Rouse-mode correlators.

4. Finite-*N* corrections

So far, we have derived the asymptotic solution of our MCT equations in the limit of large degrees of polymerization N, by retaining only the leading contribution in the expansion in the mode parameter. To find finite-N corrections, one has to go beyond the leading order, but it is difficult to explicitly work this out. On the other hand, it is obvious that finite-N corrections lead to deviations from the asymptotic (Rouse-model) results: when the normalized Rouse-mode correlator $c_p(t)$ in the α regime is fitted via a Kohlrausch function $A_p\exp[-(t/\tau_p)^{\beta_p}]$, finite-$N$ corrections lead to $A_p<1$, $\beta_p<1$, and deviations from $\tau_p\propto(N/p)^2$. Furthermore, the monomer-averaged MSD does not exhibit the square-root time dependence any longer.

[1] J. Non-Cryst. Solids **307-310** (2002), special issue of the International Discussion Meeting on Relaxations in Complex Systems, edited by K. L. Ngai, G. Floudas, A. K. Rizos, and E. Riande.

[2] M. Doi and S. F. Edwards, *The Theory of Polymer Dynamics* (Oxford University Press, Oxford, 1986).

[3] C. Bennemann, W. Paul, K. Binder, and B. Dünweg, Phys. Rev. E **57**, 843 (1998).

[4] M. Aichele and J. Baschnagel, Eur. Phys. J. E **5**, 229 (2001); **5**, 245 (2001), and references therein.

[5] A. Arbe, J. Colmenero, F. Alvarez, M. Monkenbusch, D. Richter, B. Farago, and B. Frick, Phys. Rev. Lett. **89**, 245701 (2002).

[6] A. V. Lyulin, N. K. Balabaev, and M. A. J. Michels, Macromolecules **36**, 8574 (2003).

[7] W. Paul and G. D. Smith, Rep. Prog. Phys. **67**, 1117 (2004) and references therein.

[8] J. Baschnagel and F. Varnik, J. Phys.: Condens. Matter **17**, R851 (2005).

[9] K. S. Schweizer, J. Chem. Phys. **91**, 5802 (1989); **91**, 5822 (1989).

[10] W. Paul, D. Bedrov, and G. D. Smith, Phys. Rev. E **74**, 021501 (2006).

[11] W. Götze, in *Liquids, Freezing and Glass Transition*, edited by J.-P. Hansen, D. Levesque, and J. Zinn-Justin (North-Holland, Amsterdam, 1991), p. 287.

[12] W. Götze and L. Sjögren, Rep. Prog. Phys. **55**, 241 (1992).

[13] W. Götze, J. Phys.: Condens. Matter **11**, A1 (1999).

[14] K. S. Schweizer and J. G. Curro, Adv. Chem. Phys. **98**, 1 (1997).

[15] S.-H. Chong and M. Fuchs, Phys. Rev. Lett. **88**, 185702 (2002).

[16] M. Aichele, S.-H. Chong, J. Baschnagel, and M. Fuchs, Phys. Rev. E **69**, 061801 (2004).

[17] For a fully quantitative comparison between MCT and simulation, the required static input has to be obtained with sufficiently high precision. Because of this restrictive condition, there have been only a limited number of such comparative studies. At present, they include a model for amorphous SiO_2 melts [F. Sciortino and W. Kob, Phys. Rev. Lett. **86**, 648 (2001)], a binary Lennard-Jones mixture [W. Kob, M. Nauroth, and F. Sciortino, J. Non-Cryst. Solids **307-310**, 181 (2002)], a hard-sphere mixture [G. Foffi *et al.*, Phys. Rev. E **69**, 011505 (2004)], a quasi-hard-sphere system [Th. Voigtmann, A. M. Puertas, and M. Fuchs, *ibid.* **70**, 061506 (2004), and a model for *ortho*-terphenyl [36,37].]

[18] K. Binder, J. Baschnagel, and W. Paul, Prog. Polym. Sci. **28**, 115 (2003).

[19] K. Kremer and G. S. Grest, J. Chem. Phys. **92**, 5057 (1990).

[20] J. P. Wittmer, P. Beckrich, A. Johner, A. N. Semenov, S. P. Obukhov, H. Meyer, and J. Baschnagel, Europhys. Lett. **77**, 56003 (2007).

[21] J.-P. Hansen and I. R. McDonald, *Theory of Simple Liquids*, 2nd ed. (Academic Press, London, 1986).

[22] We have explicitly compared the dynamics resulting with and without the use of the equivalent-site approximation (15) for short Gaussian chains where chain-end effects are more prominent. No substantial differences have been found.

[23] T. Vettorel, H. Meyer, J. Baschnagel, and M. Fuchs, Phys. Rev. E **75**, 041801 (2007).

[24] Without any further approximation introduced in the main text, a typical CPU time requested to solve the full matrix MCT equations (22) and (26) for the present model ($N=10$) at a temperature near the MCT critical point T_c is estimated to be of the order of one month on a Pentium IV processor with 2.80 GHz clock speed.

[25] W. Kob, M. Nauroth, and F. Sciortino, J. Non-Cryst. Solids **307-310**, 181 (2002).
[26] The regular contribution, which is not taken into account in our theory, might contain some polymer-specific (e.g., chain-length-dependent) features.
[27] For example, the long-time limit of the coherent density correlator $f(q) \equiv \phi(q,t\rightarrow\infty)$ can be determined by solving Eq. (55), and one has to solve analogous matrix equations for obtaining that of the single-chain density correlators $F^s_{ab}(q,t\rightarrow\infty)$. The solution of Eq. (55) can be found numerically by an iterative procedure $f^{(j+1)}(q)/[1-f^{(j+1)}(q)]=\mathcal{F}_q[f^{(j)}]$ starting with $f^{(0)}(q)=1$, and is obtained as $f(q)=\lim_{j\rightarrow\infty} f^{(j)}(q)$. The convergence of this iterative procedure is ruled by the spectral radius of a so-called stability matrix which can be defined in terms of the mode-coupling functional F_q [11]. The stability matrix attains the maximum eigenvalue unity at the MCT critical point T_c, and more iterations are necessary to solve Eq. (55) closer to T_c. However, this does not apply to the corresponding iterative procedure for solving the equations for the single-chain density correlators, and a much smaller number of iterations is sufficient for obtaining $F^s_{ab}(q,t\rightarrow\infty)$.
[28] P. H. Verdier, J. Chem. Phys. **45**, 2118 (1966).
[29] S.-H. Chong and W. Götze, Phys. Rev. E **65**, 041503 (2002).
[30] C. Bennemann, J. Baschnagel, and W. Paul, Eur. Phys. J. B **10**, 323 (1999).
[31] T. Franosch, W. Götze, M. R. Mayr, and A. P. Singh, J. Non-Cryst. Solids **235-237**, 71 (1998).
[32] T. Franosch, M. Fuchs, W. Götze, M. R. Mayr, and A. P. Singh, Phys. Rev. E **55**, 7153 (1997); M. Fuchs, W. Götze, and M. R. Mayr, *ibid.* **58**, 3384 (1998).
[33] C. Bennemann, J. Baschnagel, W. Paul, and K. Binder, Comput. Theor. Polym. Sci. **9**, 217 (1999).
[34] J. S. Shaffer, J. Chem. Phys. **101**, 4205 (1994).
[35] M. Guenza, Phys. Rev. Lett. **88**, 025901 (2001).
[36] A. Rinaldi, F. Sciortino, and P. Tartaglia, Phys. Rev. E **63**, 061210 (2001).
[37] S.-H. Chong and F. Sciortino, Phys. Rev. E **69**, 051202 (2004).
[38] M. Aichele, Ph.D. thesis, Universität Mainz, 2003, http://archimed.uni-mainz.de/pub/2003/0084
[39] B. Farago, A. Arbe, J. Colmenero, R. Faust, U. Buchenau, and D. Richter, Phys. Rev. E **65**, 051803 (2002).
[40] S.-H. Chong and F. Hirata, Phys. Rev. E **57**, 1691 (1998).
[41] D. Chandler, J. D. McCoy, and S. J. Singer, J. Chem. Phys. **85**, 5971 (1986).
[42] We confirmed from our independent computer simulations performed for a bead-spring model similar to the one studied here that the wave vector at which the high-temperature collective dynamics is slowest does not shift with N.
[43] U. Grenander and G. Szegö, *Toeplitz Forms and Their Applications* (University of California Press, Berkeley, 1958).
[44] J. P. Wittmer, P. Beckrich, H. Meyer, A. Cavallo, A. Johner, and J. Baschnagel, Phys. Rev. E **76**, 011803 (2007).